DIGITAL TERRAIN ANALYSIS IN ILWIS

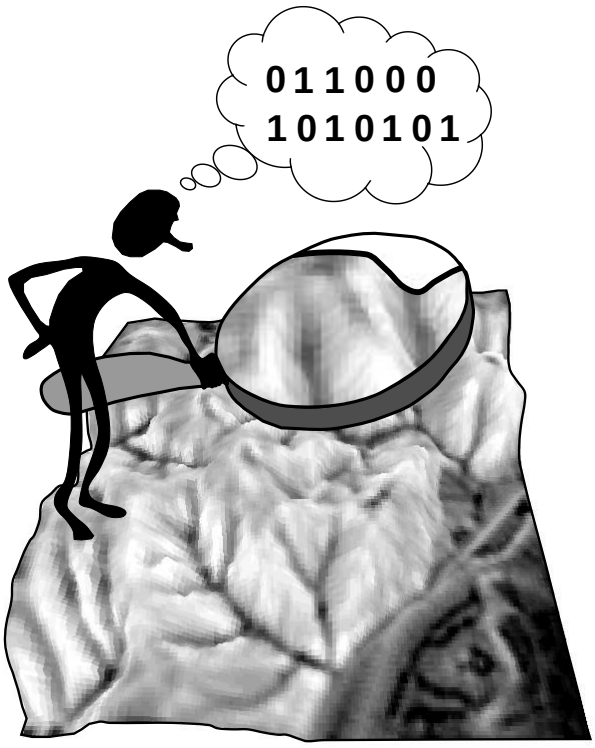

T. Hengl, S. Gruber and D.P. Shrestha

August 2003

Digital Terrain Analysis in ILWIS

Lecture notes and user guide

TOMISLAV HENGL
Department of Earth Systems Analysis, International Institute for Geo-information Science and Earth Observation (ITC), P.O. Box 6, 7500 AA Enschede, Netherlands.
E-mail: hengl@itc.nl;

STEPHAN GRUBER
Glaciology and Geomorphodynamics group, Department of Geography, University of Zürich, Winterthurerstr. 190, CH-8057 Zrich, Switzerland;
E-mail: stgruber@geo.unizh.ch;

DHRUBA PIKA SHRESTHA
Department of Earth Systems Analysis, International Institute for Geo-information Science and Earth Observation (ITC), P.O. Box 6, 7500 AA Enschede, Netherlands.
E-mail: shrestha@itc.nl;

Supplementary materials, full colour visualisations, ILWIS scripts and datasets available at
`http://www.itc.nl/personal/shrestha/DTA/`

Foreword

This lecture notes are intended for all ITC students, primarily participants of the Natural Resources (NRM), Water Resources (WREM) and Earth Resources (EREG) programmes. Other people interested in the application of digital terrain analysis and all current and potential users of Integrated Land and Water Information System (ILWIS) package [71] are also welcome. After completion of the course students are able to employ and critically reflect existing terrain analysis tools and to implement own algorithms in ILWIS or similar software. A reader should be familiar with the basic GIS raster techniques and has a background in physical geography or similar earth sciences dealing with terrain. Students should also be familiar with these terms and concepts: raster/vetcor GIS, pixel size/scale, GIS operations and ILWIS scripts. The following chapters/books are suggested for beginners:

- Chapt. 5, 7 and 8. in Burrough, P.A. and McDonnell, R.A., 1998. Principles of geographical information systems. Oxford University Press, Oxford, 327 pp.
- Chapt. 9, 10 and 12. in Unit Geo Software Development, 2001. ILWIS 3.0 Academic user's guide. ITC, Enschede, 520 pp.

To review the content of this document, students should also refer to the the following literature:

- Lane, S.N., Richards, K.S. and Chandler, J.H., 1998. Landform monitoring, modelling and analysis. John Wiley and Sons, 466 pp.
- Wilson, P.J. and Gallant, C.J. (Editors), 2000. Terrain analysis: principles and applications. John Wiley and Sons, Ltd., New York, 303 pp.
- Weibel, R. and Heller, M., 1991. Digital terrain modelling. In: D.J. Maguire, Goodchild, M.F. and Rhind, D.W. (Editor), Geographical information systems. Longman, London, pp. 269–297.
- Moore, I.D., Grayson, R.B. and Ladson, A.R., 1991. Digital terrain modelling: a review of hydrological, geomorphological, and biological applications. Hydrological Processes, 5(1): 3–30.

The materials consist of two parts: theoretical introduction and user guide developed using a small case study. You can download the datasets and scripts and see dynamic visaulisations of the error propagation at `http://www.itc.nl/personal/shrestha/DTA/`.

Note that some scripts are not full operational and some contain unresolved bugs within ILWIS. If you discover such problems, feel free to contact authors or report a bug directly to ILWIS development team.

We would like to thank the ILWIS team for their support, namely J.H.M. Hendrikse for suggestions about the scripts and C. Hecker, software tester for reporting and processing bugs we discovered during the development of applications. Principles developed in this lecture note will serve as a basis for the development of a special module for terrain analysis within ILWIS. We would also like to thank Dr. K. Tempfli (EOS department, ITC), who has been teaching interpolation techniques and technical and technological issues related to the production and use of DEM. He produced two lecture notes used internally at ITC: "Topography and Orthophotography" and "Interpolation and filtering", which we referred to many times.

In Enschede, July 2003

INTERNATIONAL INSTITUTE FOR GEO-INFORMATION SCIENCE AND EARTH OBSERVATION

ENSCHEDE, THE NETHERLANDS

Contents

Chapter 1

Theory

1.1 Key concepts

1.1.1 What is Digital Terrain Analysis?

The process of quantitatively describing terrain is known as *Digital Terrain Analysis* (DTA in the further text) [14]. Common synonyms are geomorphological analysis [41], landform parameterization and land surface analysis [61]. A digital terrain model [44], also referred to as the Digital Elevation Model (DEM) is a digital representation of earth's topography, i.e. an elevation map[1]. DEM can be used to derive topographic attributes [76], geomorphometric parameters [41], morphometric variables [61] or terrain information in general [42]. We make a distinction between the DTA and the term *Digital Terrain Modelling* (or DTM), which also refers to the generation of terrain data. In order to avoid terminological confusion, we use the term DTM to describe a set of interpolation/filtering techniques used to derive the topographic surface, and the term DTA for a set of techniques used to derive terrain parameters. Note that these are our arbitrary definition, which might differ from the other literature. Finally, the following terminology is used consistently throughout the lecture notes:

- DEM — Digital elevation map, i.e. representation of the Earth's surface topography.
- DTM — a set of techniques used to derive or present a DEM.
- DEM filtering — a set of techniques used to improve the geomorphic resemblance of a DEM.
- Terrain analysis or parameterization — Terrain parameterization is a set of techniques used to derive terrain parameters from a DEM, i.e. a process of quantifying the morphology of a terrain. Terrain analysis (DTA) is used as a general term used for derivation of terrain parameters and their application.
- Terrain parameter — parameter (maps or images) derived from a DEM using DTA, e.g. slope.
- Topography or relief — is the shape or configuration of the land, represented on a map by contour lines, hypsometric tints, and relief shading.

1.1.2 The key DTA literature

To list all applications of DTA would require probably a whole chapter or maybe a whole book. Instead, we will only give some key references to the most recent overviews of DTM and DTA techniques. A concise introduction to DTM techniques is given by Weibel and Heller [74]. Moore et al. [50] give an overview of DTA applications in hydrological, geomorphological and biological applications and lists terrain analysis programs for the environmental sciences. Fels [17] gives a detailed comparison of DTA techniques for mapping potential vegetation. Franklin [21] gives another review of predictive vegetation mapping

[1] A set of points or grids in cartesian space attributed with elevation values that approximates the Earth's surface. Note that the contour data or any other sampled elevation datasets are not DEMs! A DEM implies that elevation is available continuously at each location in the study area.

based on terrain analysis. Woo [79] discusses different interpolation, filtering and visualisation DTA tools. Mitas and Mitasova [45] compared various interpolation techniques for optimal DTM. Lane et al. [38] give a review of most recent methodological developments of DTM methods in geomorphology. Wilson and Gallant [76] produced a comprehensive overview of DTA methods, including an overview of applications to geomorphology, hydrology, soil and vegetation mapping. The latest book is probably the state-of-the-art reference of DTA. Unfortunately, it focuses on the applications with the software package TAPES or Terrain Analysis Programs for the Environmental Sciences [22] and therefore serves more as a user manual.

There has been an increasing interest in the use of relief data in the last decade accompanied by a growing availability of DEMs. Terrain parameters are inexpensive and available in continuous fashion and can therefore be used to replace part of the expensive field sampling. DTA has been successfully used to predict distribution of soil properties [49, 3, 24], model depositional/erosional processes [47] or improve vegetation mapping [4]. Landform parameters can be used to derive soil-landscape elements and provide more objective basis for production of soil maps [34]. Other authors have attempted to directly derive soil classes from the landscape variables [67, 66]. Recent developments include use of automated methods to detect landform facets using unsupervised fuzzy-set classifications [6]. These can then be applied even in the areas of lower relief to enhance crop production using site-specific management [40].

1.1.3 DTA Software

Young [81] was among the first who developed a computer algorithm for calculation of slope, aspect and curvatures using the matrix calculations. Other early computer applications for DTA are given by Horn [31] and Pennock et al. [52]. Martz and de Jong [43] developed a computer algorithm to calculate the hydrological parameters. Since the 90's, DTA has been implemented in many general GIS packages. Most of these, such as ArcGIS 8.x, IDRISI, ERDAS or ILWIS, can only run simple filter operations and derive e.g. slope, aspect and hillshading maps. More advanced DTA tools, e.g. for hydrologic modelling, are incorporated within the ArcInfo Grid module. For example, the ANUDEM interpolation method with drainage enforcement [33] is implemented in the TOPOGRID command of the ArcInfo 8 GIS [13]. Another option is use of the Topoview, the ArcView extension that calculates incoming solar radiation (insolation) based upon DEMs [26].

There are also a number of standalone terrain analysis packages available on the market today. For example the TopoMetrix [70], which can be used to derive aspect, slope, Terrain Shape Index (TSI), terrain concavity/convexity, catchment area, wetness index, shaded relief and other parameters. Shary et al. [61] developed a commercial package called Analytical GIS Eco, which derives some twenty morphometric terrain parameters. Somewhat more extensive is the LandLord [19], which offers various operations from DEM interpolation to derivation of gradient, aspect, curvatures, specific catchment area, topographic and stream power indices. The Environmental Modeling Research Laboratory at the Brigham Young University (EMRL) developed a set of tools for hydrological analysis grouped in three packages: Groundwater Modeling System (GMS), Surface-water Modeling System (SMS), and Watershed Modeling System (WMS) [12]. From these three, especially the WMS module

belongs to the domain of DTA more closely. It can be used for automated watershed and sub-basin delineation, geometric parameter computation, hydrologic parameter computation and visualization of results.

Probably the most detailed set of standalone terrain analysis software tools are developed at the Centre for Resource and Environmental Studies in Canberra (CRES[2]). Different modules of it, such as EROS [75] used for erosion modelling or SRAD used for solar radiation modelling, have been especially interesting for environmental applications. CRES also distributes the ANUCLIM [32], which uses meteorological data (points) and DEM to produce estimates of monthly mean climate variables and bioclimatic parameters.

The freely available terrain analysis packages are TARDEM and TauDEM, developed at the Utah Water Research Laboratory [64]. These can be used for mapping of channel networks and watersheds. Conrad [7] developed a package called "Digitales Gelände-Modell" or DiGeM, which can be downloaded from the website of Department for Physical Geography, University of Göttingen. This powerful application can be used to derive slope, aspect, curvatures, catchment area, topographic indices, drainage networks and visualise the results in 3D space. Woo [80] developed Landserf, a freely downloadable Java application that can be used to automatically extract morphometric parameters and landform features. Number of terrain analysis procedures have also been implemented in the open source GRASS (Geographic Resources Analysis Support System) GIS software, especially for the purpose of hydrological modelling and erosion mapping [48].

1.1.4 DEM data sources

At present, there are five main sources of the elevation data:

1. Ground surveys;
2. Airborne photogrammetric data capture;
3. Existing cartographic surveys (e.g. topo-maps);
4. Airborne laser scanning and
5. Stereoscopic or radar-based satellite imagery.

These DEM collection methods can be compared considering four aspects: (a) price, (b) accuracy, (c) sampling density and (d) pre-processing requirements (Table 1.1). Traditionally, the elevation data has been collected by land-surveyors from ground surveys or by semi-automated digitising using stereoplotters. This is the most accurate but also the most expensive data collection method. The most recent developments consider automated stereo-image matching, use of laserscanning and remote sensing imagery, either with stereoscopic overlap (SPOT, ASTER) or interferometric imagery. Note that in the case of elevation data derived from the remote sensing sources, the sampling density is closely related to the ground resolution.

From the above-mentioned techniques, laserscanning seems to be the most accurate method with the highest sampling density. Moreover, in the case of laserscanning, both

[2]The same Institute developed the previously mentioned TAPES.

Table 1.1: Typical elevation accuracy of different data sources used to derive DEMs.

Collection method	Main characteristics	Some examples of used systems	Typical DEM accuracy
Ground survey	highest accuracy; small sampling density; high costs;	DGPS systems	≤1 m
		tacheometry (total station)	1 mm - 1 m
		levelling systems	≈1 mm
Stereoscopic imagery	high sampling density; can be semi- or fully automated; problems with vegetation;	aerial photography	0.1–1 m
		satellite imagery (SPOT, ASTER)	10 m (20 m)
Laser scanning	laser scanner is placed in the airplane which is GPS navigated; the raw data require filtering and resampling before it can be used; it can penetrate tree foliage and record both surface of the vegetation cover and ground;	airborne laserscanning (LIDAR)	≈0.2–1.0 m
Radar imagery (Interferometric)	the lowest costs per km^2; requires ground control data; complex processing;	airborne SAR (Synthetic Aperture Radar)	≈0.5–2 m
		spaceborne (ERS, SRTM)	10 m (25 m)

object surface and ground surface can be recorded, so that the elevation data is better defined as the *Digital Surface Models*[3] (DSM). A comparison of several elevation surfaces can then be used to map three heights or estimate volume of objects. Laserscanning has already been applied for mapping buildings, power lines, open pits, surface textures and even waves in the water [69]. The second highly cost-effective new technique is the airborne and spaceborne interferometric radar system, which can be used to accurately derive both the land cover and terrain data [10]. Typical elevation Root Mean Square Error $RMSE(z)$, achieved with the use spaceborne interferometric images ranges from few to ten meters [82].

DEMs are increasingly available on the market today. Many countries already provide elevation grids at course resolutions ($>$ 250 m) and at a commercial price. Free source of elevation data with the global coverage is the global digital elevation map with a horizontal grid spacing of 30 *arc* seconds, which is approximately 1×1 km. It is derived from several raster and vector sources of national topographic information and is available via the website of the US Geological Survey [72].

On February 2000, the SRTM (Shuttle Radar Topography Mission) radar system gathered topographic data over approximately 80% of the land surfaces of the Earth, creating the

[3]There can be several surfaces observed, not only the Earth's surface.

first-ever near-global data set of land elevations of 1 *arc* second (about 30 meters) and 3 *arc* seconds (about 90 meters) ground resolutions. In the USA, this data have been released to the public and are available at the US Geological Survey's EROS (Earth Resources Observation Systems) Data Center for download via FTP [51]. Data for areas outside the USA (not yet released for public distribution) can be requested from the NASA or other commercial companies (e.g. via German Aerospace Center (DLR) at `http://www.dfd.dlr.de/srtm/`).

1.2 Modelling terrain

1.2.1 DEM data structures

In a GIS environment, a DEM is commonly modelled and visualised using two main data structures: (1) rectangular grid or elevation matrix (GRID) and (2) Triangulated Irregular Network (TIN) [53]. The GRID DEM is typically stored as a raster map (or image), where each pixel carries the information on elevation or terrain parameter. The TIN DEM is based on the triangular elements with their vertices at the sample points. The advantage of TIN DEM compared to the GRID DEM is that it can incorporate structural features such as peaks, slope breaks and conic pits, and by some is considered a more accurate structure for terrain parameterisation especially when contour data is used [29]. Although the gridded DEM-data model is non-adaptive and commonly over-samples in low-relief areas and under-samples in high-relief areas, it is somewhat more attractive than the TIN DEM due to a simple data structure and high possibilities of GIS operations [78]. It is easier to manipulate, process and integrate it with other GIS data, especially in the DTA applications and has been used as the primary structure in ILWIS and other similar GIS packages.

1.2.2 Interpolation

If the elevation data is sampled at point locations or digitised from the contour lines, a primary DEM generation concern is the interpolation method. These range from nearest point, triangulation, inverse distance, minimum curvature and splines up to different kriging techniques [78]. The DEM interpolation methods can be grouped by the two aspects: (a) smoothing effect, and (b) proximity effect. By a smoothing effect the interpolator can be either exact or approximate and by the proximity effect, it can be either global or local. An exact interpolator preserves the values at the sampled data points and is usually based on the values in the nearest neighbourhood. Kriging techniques, for example, usually[4] over-smooths the original values and can depend on the values from a larger neighbourhood.

A search for optimal DEM interpolation method has been of interest for quite some time. Most probably there is no 'best' universal interpolator, which is clearly superior and appropriate to all applications [74]. Mitas and Mitasova [45], however, showed that the quality of a DEM depends on how good is smoothness and tension described and how good are streams and ridges incorporated. They finally suggested the regularized splines with tension algorithm [46] as an 'optimal' DEM interpolator. This algorithm has been implemented in the previously mentioned GRASS GIS and ANUSPLIN software (distributed by CRES).

[4] Kriging preserves the original values only if the nugget equals zero.

Another flexible solution for interpolation of contour data is the minimum curvature method [20], which is applied in SURFER [62]. A DEM with a connected drainage structure and realistic presentation of streams and ridges can be produced using the TOPOGRID command in ArcInfo 8 for example. The method is explained in detail by Hutchinson [33].

Rule 1 Elevation is a non-stationary, non-periodic and fractal feature. In many cases, however, it can be approximated using a contiguous and smooth surface.

If the density and quality of sampled elevations is high, a local and exact interpolator (e.g. inverse distance or splines with very low tension) is considered to be most appropriate. In fact, the surface topography is non-stationary[5] and non-periodic[6] feature and therefore we should always aim at preserving the original values at sampled points [74]. In addition, an algorithm that incorporates the secondary information (pits, streams, ridges, scarps, fault lines) is recommended for interpolation of sampled elevation data.

Another intrinsic property of elevation is its fractal nature. This has two implications: (a) there has to be some discretisation at the horizontal and vertical scales and (b) the same terrain parameters will look different for the same study area if derived at different scales, i.e. by using different grid-sizes, vertical accuracy and precision. The fractal property of terrain also means that we can find topography at kilometer, meter and millimeter scales. Although in geomorphology relief is commonly classified as high (e.g. mountain) or low (e.g. terrace), even if the terrain is of low relief (plain), the visual impression of topography (relative topography) will be distinct if both the vertical accuracy and precision are high.

Rule 2 Absolute relief is a measure of the relief significance. Relative relief is a measure of how good is the topography sampled — even if the terrain is of low relief (plain), the topography will be distinct if both the vertical accuracy and precision are high.

1.2.3 DEM quality issues

The quality of a DEM is a measure of how accurate elevation is at each pixel (absolute accuracy) and how accurately is the morphology presented (relative accuracy). Several factors play an important role for quality of DTA products [18]:

[5] Statistical term — it means that elevation (as a spatial variable) does not have constant internal properties, such as mean, variance, autocorrelation etc. over an area. This means that if we make sub-samples of an area, we should expect to measure different internal properties.

[6] Non-periodic feature is a feature with an irregular structure. For example, an amorphous crystal has non-periodic shape.

- terrain roughness,
- sampling density (elevation data collection method),
- grid spacing or pixel size,
- interpolation algorithm,
- vertical resolution and
- terrain analysis algorithm.

Interpolation of digitised contour lines using the linear interpolator will typically show artefacts in the slope and aspect maps [5, p. 127]. The problem is that some DTA algorithms used in the calculation of terrain parameters are more sensitive to the relative change of neighbouring elevation values than their absolute values. The most typical artefacts are so called "padi" or "rice" terraces or cut-offs, ghost lines and tiger strips [5]. The padi terraces are formed when all rays of the interpolation algorithm finds the same contour value in the neighbourhood. In these areas calculation of aspect map or CTI and similar parameters gives undefined values due to the division by zero. These artefacts may not be visible in the original DEM map, but will often be clearly visible as undefined values in terrain parameters. The artefacts are even bigger problem for calculation of hydrological parameters.

Errors are especially common for terrain parameters derived using the higher order derivatives (curvatures), aspect map and hydrological parameters [78]. With the increase of pixel size, spatial prediction will be less discernible, while decreased vertical precision will typically show more erratic values [68]. The finer grid resolutions and flexible algorithms often give more satisfactory for the end-users [77]. Accuracy of DEM-derived hydrological data is directly related to DEM vertical resolution and terrain roughness. In the areas where the slope is less than four degrees, the hydrological parameters are usually unreliable [63].

Rule 3 Absolute accuracy — is the RMS error between the true elevations and DEM values.
Vertical precision — is the smallest measurement unit, or rounding number; also called "vertical resolution". This number is typically smaller than the absolute accuracy.
Relative accuracy (plausibility or fidelity of a DEM) — accuracy of presenting the shapes; summary RMS error of terrain parameters. It is less a function of absolute accuracy of elevation values than of how well and how realistically the landscape shapes and processes are presented.

1.2.4 Selecting the suitable grid size and vertical precision

The first step in optimising the production of terrain parameters is to select a suitable grid size and vertical resolution. Although often neglected, the distinction between the

vertical resolution, vertical accuracy, scale and grid size is important for the successful terrain modelling. The optimal grid size for DTA is a compromise between the accuracy of terrain parameters and cost-effectiveness. In general, an increase in the detail in the DEM will also mean more accurate terrain parameters. This increase, however, depends on the general variability of the landscape. For example, a generally simple and smooth landscape might not need a fine resolution DEM. As a rule of thumb, the pixel size should be smaller than the average distance at which a distinct change in landform occurs. Imagine a one-dimensional topography with specific number of inflection points[7] (Fig. 1.1). Theoretically speaking, the largest grid size should be at least the average spacing between the inflection points:

$$p_{\max} \leqslant \frac{l}{n\left(\delta z\right)} \tag{1.1}$$

where l is the lenght of a transect and $n\left(\delta z\right)$ is number of inflection points observed.

In this example (Fig. 1.1) there are 20 inflection points in DEM with an average spacing of 0.8 m between them. Hence, a grid size of at least 0.8 m is recommended. However, the selection of the most suitable grid size is not as simple as it seems. Because topography is a fractal feature, its roughness is practically immeasurable. Hence, the number of inflection points also depends on the size of the argument (Δx), which is somewhat similar to the concept of the grid size. This means that we can estimate number of inflection points only after we define a certain grid size (the 'chicken-egg' problem)! Therefore, no absolute optimal pixel size exists. There is only a suitable grid size for a given scale of research.

In the case of contour data, the suitable grid size can be estimated from the total length of contours. Here, the contours present mapped changes (inflection points) of elevation[8]. As a rule of thumb, the grid resolution should be at least half the average spacing between the contours:

$$p = \frac{A}{2 \cdot \sum l} \tag{1.2}$$

where A is the total size of the study area and $\sum l$ is the total cumulative length of all digitised contours. Note that the we use somewhat lower number (half) because we know that the contours do not typically record hilltops and valley bottoms.

Alternatively, the suitable grid resolution can be estimated using the cartographic rules. According to Tempfli [65], the grid resolution should be optimally the maximum graphic resolution of lines shown on the maps, i.e. 0.4 mm at map scale. This number is somewhat higher than the maximum location accuracy standard, i.e. 0.25 mm at map scale, according to the definition of Vink [73]. Another option is to choose the pixel size that corresponds to the minimum resolution of application, e.g. soil mappers typically inspect representative blocks of land of size of at least 10×10 m [58]. Often the selection of the pixel size is limited

[7] Inflection point is a location at which the second derivative of a function (z) changes sign, i.e. location at which a function changes from being convex to concave, or vice versa.

[8] Note that the density of contour lines is much lower since the contours typically will not capture ridges and valley bottoms.

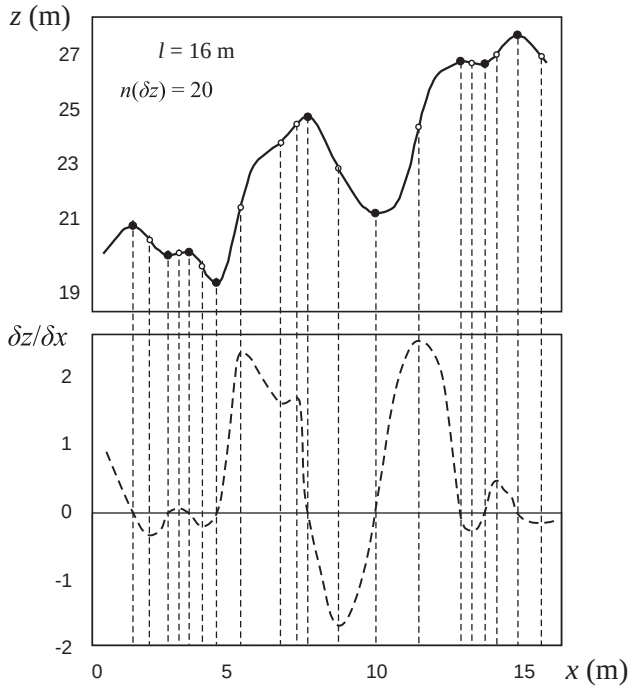

Figure 1.1: Schematic example for selection of the suitable grid size: hypothetical variation of elevation (z) and the first derivative; $n\,(\delta z)$ is the total number of inflection points and l is the length.

due to the processing power and scale of application. For regional and national level studies, a high resolution DEM is unrealistic.

Rule 4 A suitable grid resolution for DTA is (at least) half the average spacing between the digitized contours.
The suitable grid resolution can also be related to the map scale — the smallest spacing between the contours is e.g. 0.4 mm at map scale.

Information on contours can also be used to estimate the accuracy of elevation measurements $RMSE(z)$ and suitable vertical precision of a DEM. In the case the DEM is derived from the contour data, $RMSE(z)$ can be estimated from the contour interval h and local slope [39]:

$$RMSE(z) = B \cdot h + RMSE(xy) \cdot \tan\beta \tag{1.3}$$

where B is empirical number (commonly used values are within the 0.16–0.33 range), $RMSE(xy)$ is the (empirical) planimetric error and β is the local slope [54]. For the 1:50 K scale, the planimetric error is about 10 m. In the case of padi terraces, the slope equals zero so the $RMSE(z)$ can be estimated directly from the contour interval. If the contour interval is 10 m and $B = 0.25$ then we can estimate the $RMSE(z)$ to be 2.5 m in flat terrains. One should also take into account that the cartographers usually use different contour intervals in relatively flat terrains and different in mountainous terrains.

Although, in principle, any small number can be used for vertical precision of the DEM, this number can also be estimated statistically. The vertical precision of the DEM can be compared to the selection of the optimal histogram bin size. For a given data set of size N, the bin width W is commonly estimated using the unbiased estimation of the probability density function [36]:

$$W = 2 \cdot IQR \cdot N^{-\frac{1}{3}} \tag{1.4}$$

where W is the bin width, IQR is the interquartile range (the 75th percentile minus the 25th percentile) and N is the number of available samples. Hence, in the case of contour data, the vertical precision can be estimated using:

$$W = h_{\min} \cdot N^{-\frac{1}{3}} \tag{1.5}$$

where $h_{\min}$ is the smallest contour interval and N corresponds to the number of times a surveyor places a contour line of the same designation (elevation class). In this case N is unknown. It can be, however, estimated from the planned number of bins ($2^{(b-1)}$). This means that if we want to describe the vertical resolution with 10 bins (about 500 realisations) and if the smallest contour interval is 2 m, than the vertical precision should be 0.25 m. This means that, as a rule of thumb, the vertical precision should be at least 1/8th of the smallest contour interval to accurately estimate the probability density function. Note that we used the smallest contour interval because it controls the overall precision.

In the general case, the vertical resolution can be estimated directly from the $RMSE(z)$ and desired number of bins:

$$W = 3.49 \cdot RMSE(z) \cdot N^{-\frac{1}{3}} = 3.49 \cdot RMSE(z) \cdot 2^{-\frac{b-1}{3}} \tag{1.6}$$

Note that the Eq. 1.6 can be also used for an optimal display histogram of a TP. In that case, N corresponds to the total number of grids.

1.2.5 Improving the plausibility of DEM

For DTA, it is more important how does the DEM resemble the shapes and flow potential. Therefore, it is probably more appropriate to use the term *geomorphological plausibility* to denote the quality of a DEM [60]. Because a good presentation of shapes is more important than the actual values in the DEM, a set of additional filtering methods can be applied to adjust the original DEM values. The process of DEM filtering can be considered as a set of steps, which can be applied iteratively to produce a realistic DEM, i.e. to minimise the errors in terrain parameters. We recommend (at least) three DEM filtering steps prior to derivation of terrain parameters [27]:

1. Reduction of padi terraces;
2. Reduction of outliers and
3. Incorporation of water bodies.

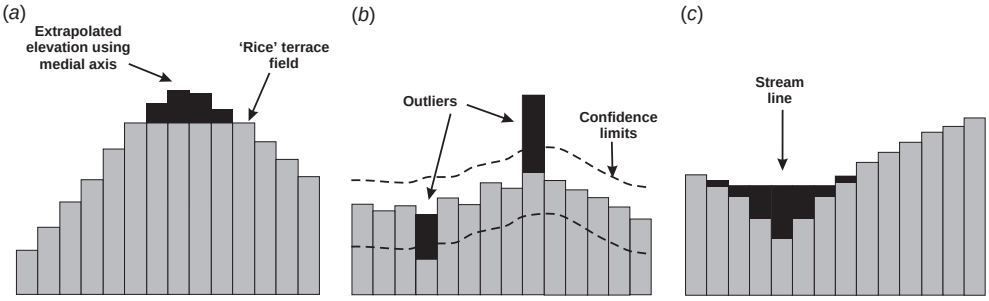

Figure 1.2: Schematic examples of DEM fitlering using cross-sections: (a) reduction of padi terrace fields; (b) reduction of outliers and (c) adjustment of the elevation using drainage lines. Black-coloured strips indicate the change in elevation values.

Reduction of padi terraces

First step in improving the DEMs derived from the contour data is to account for features not shown by the contours such as break-lines indicating ridges or valley bottoms (Fig. 1.2a). This can be achieved by digitizing supplementary contour lines and spot heights indicating small channels, hilltops and ridges that are not indicated on the original topographic maps but can be inferred. Thorough analysis and removal of padi terraces and checking of the generated new DEM, however, can be a very time-consuming task. We therefore recommend use of automated detection of medial axes (see user guide section 2.2 on 31). At the location of the padi terraces, the medial axes can be detected using a distance operation from the bulk contour data [55]. The new elevation is assigned to the medial axes between the closed contours by adding or subtracting some threshold elevation value, e.g. standard deviation of the elevation values:

$$z_i^+ = \begin{cases} z_i + RMSE(z) & \text{if} \quad e = \text{terrace} \quad \text{and} \quad \tau = \text{convex} \\ z_i - RMSE(z) & \text{if} \quad e = \text{terrace} \quad \text{and} \quad \tau = \text{concave} \\ z_i & \text{otherwise} \end{cases} \tag{1.7}$$

where z_i^+ is the filtered elevation value, $RMSE(z)$ is the estimated accuracy of elevation measurements, the elevation map is denoted as z or DEM, terrain parameters are denoted as τ or TP and errors are denoted as e, z_i is the elevation value at ith grid location $(z_1, z_2, ..., z_n)$ and n is the number of pixels in a map.

Reduction of outliers

The outliers are small, very unprobable features, which could have happen due to the gross error in the data collection method (very common for remote-sensing based instruments) or interpolation algorithm (Fig. 1.2b). The outlier7s are reduced by calculating a probability to find a certain value within the neighbourhood [16]. Here, the original elevation is compared with the value estimated from the neighbours:

$$\delta_i = \hat{z}_i^{NB} - z_i \tag{1.8}$$

where δ_i is the difference between the original and estimated value and $\hat{z}_i^{NB}$ is the elevation[9]

A statistically sound method to estimate the central value from the neighbouring pixels is to use the spatial dependence structure, i.e. predict the central value by kriging [16]. In a 3×3 window environment, there are only two types of distances (assuming the isotropic variation) — in the cardinal (2,4,6,8) and diagonal directions (1,3,7,9) (see also Fig. 1.4). Hence, the predictions are made by:

$$\begin{aligned}\hat{z}^{NB} &= w_{\mathrm{B}} \cdot [z_{NB1} + z_{NB3} + z_{NB7} + z_{NB9}] \\ &+ w_{\mathrm{A}} \cdot [z_{NB2} + z_{NB4} + z_{NB6} + z_{NB8}]\end{aligned} \tag{1.9}$$

where z_{NB} is the local neighbourhood. In a general case (k×k window), the predictions are made by:

$$\begin{aligned}\hat{z}^{NB} &= \sum_{c=1}^{k^2} w_c \cdot z_{NBc} \\ \sum_{c=1}^{k^2} w_c &= 1\end{aligned} \tag{1.10}$$

where w_c is the weight at cth neighbour and $w_\times$ is the weight at the central pixel, so that $w_\times = 0$ and $\times = \frac{k^2+1}{2}$. Note that in the case of anisotropy, different weights can be used in different directions. The (kriging) weights are solved using the covariance function and relative distances between all pixels. For example, in the 3×3 window environment [35]:

$$\mathbf{w} = \begin{bmatrix} w_1 \\ w_2 \\ w_3 \\ w_4 \\ w_6 \\ w_7 \\ w_8 \\ w_9 \\ \mu \end{bmatrix} = \mathbf{C}^{-1} \cdot \mathbf{c}; \qquad \mathbf{c} = \begin{bmatrix} C_{1,5} \\ C_{2,5} \\ C_{3,5} \\ C_{4,5} \\ C_{6,5} \\ C_{7,5} \\ C_{8,5} \\ C_{9,5} \\ 1 \end{bmatrix} \tag{1.11}$$

[9] You can also use this method to filter outliers in terrain parameters.

where $\mathbf{w}$ is a vector of weights, $\mathbf{c}$ is a vector of covariances from all neighbouring pixels to the central pixel, m is the Lagrange multiplier and $\mathbf{C}$ is the matrix of covariances of size 9×9 (central pixel is omitted) estimated between the ith and jth location:

$$\mathbf{C} = \begin{bmatrix} C_{1,1} & \cdots & C_{1,4} & C_{1,6} & \cdots & C_{1,9} & 1 \\ \vdots & \ddots & & & & \vdots & \vdots \\ C_{4,1} & & & & & C_{4,9} & \\ C_{6,1} & & & & & C_{6,9} & \\ \vdots & & & & \ddots & \vdots & \vdots \\ C_{9,1} & \cdots & C_{9,4} & C_{9,6} & \cdots & C_{9,9} & 1 \\ 1 & \cdots & & & \cdots & 1 & 0 \end{bmatrix} \tag{1.12}$$

The prediction by kriging requires modelling of the spatial dependence structure. In the case of elevation, which is often a spatially contiguous variable [74], spatial variation can be modelled by using an unbounded semivariogram model such as the exponential model:

$$C(\lambda) = \begin{cases} C_0 + C_1 & \text{if} \quad \lambda = 0 \\ C_1 \cdot \left[e^{-\left(\frac{\lambda}{R}\right)} \right] & \text{if} \quad \lambda > 0 \end{cases} \tag{1.13}$$

or a bounded model such as the spherical model:

$$C(\lambda) = \begin{cases} C_0 + C_1 & \text{if} \quad \lambda = 0 \\ C_1 \cdot \left[1 - \left(1.5 \cdot \frac{\lambda}{R} - 0.5 \cdot \left\{ \frac{\lambda}{R} \right\}^3 \right) \right] & \text{if} \quad \lambda > 0 \end{cases} \tag{1.14}$$

where λ is the Euclidian distance between a point pair and C_0, C_1, R are the estimated variogram parameters. Note that because we are only interested in the local spatial dependence, only first 10–15 surrounding pixels are considered for semivariogram modelling.

The difference between estimated and true value is calculated for each pixel to derive overall average and standard deviation ($\bar{\delta}$ and s_δ). Assuming a Gaussian distribution, Student's t test is used to standardise the differences by:

$$t_i = \frac{\delta_i - \bar{\delta}}{s_\delta}; \qquad i = 1, ..., n \tag{1.15}$$

From the t value (Eq. (1.15)), we can derive the normal probability $p(t)$, which can be used as a weight function. The smoothed DEM can then be derived as a weighted average from the original DEM and estimated elevations:

$$z_i^+ = p(t_i) \cdot z_i + [1 - p(t_i)] \cdot \hat{z}_i^{NB}; \qquad p(t) \in [0, 1] \tag{1.16}$$

where z^+ is the filtered elevation map and $p(t)$ is the probability of exceeding a value estimated from the neighbours using the spatial dependence structure. The averaged elevation will be somewhat smoothed after the filtering for outliers. However, weak smoothing of elevation prior to terrain analysis is often recommended [15].

Incorporation of water bodies

The third step in improving the geomorphic plausibility of a DEM is adjustment of elevations by incorporating the additional information, e.g. map of streams, water bodies and small channels (Fig. 1.2c). In ILWIS, the streams (lines) and water bodies need to be first rasterized. A distance map (buffer) can then be used to calculate the DEM adjustment. We recommend the following formula:

$$\begin{aligned} \Delta z_i &= \left(\frac{p}{p+d_i}\right)^{\varphi} \cdot H \\ \Delta z_i &\in [0, H] \\ z_i^+ &= z_i - \Delta z_i \end{aligned} \tag{1.17}$$

where Δz_i is the adjustment of elevation, p is the pixel size, H is the maximum elevation difference, d_i is the distance from streams map and φ is the adjustment factor. This means that the original DEM will 'sink' proportionally to the distance from the streams.

1.2.6 Reduction of errors using error propagation

Due to a high sensitivity of terrain analysis algorithms to local conditions, any single realisation represents only one view on terrain morphology. This is especially important for the calculation of hydrological parameters and curvatures where we are more interested in the general picture of the processes. Even for the perfectly adjusted DEM, the location of the stream network can differ up to 3–4 cells from the true location [5]. A statistically robust approach to reduce the errors in terrain parameters is to average a set of possible realisations given the uncertainty in elevation values [6, 57]. This is also referred to as the Monte Carlo method of error propagation [28]. The elevation values can be simulated using the inverse normal probability function [2]:

$$\begin{aligned} z_i^* &= z_i + RMSE(z) \cdot \sqrt{-2 \cdot \ln(1-A)} \cdot \cos(2 \cdot \pi \cdot B); \quad i = 1, ..., n \\ A, B &\in [0, 1) \end{aligned} \tag{1.18}$$

where A and B are the independent random numbers within the $0 - 0.99\ldots$ range, z_i is the original value at ith location, is the simulated elevation with induced error and $RMSE(z)$ is the standard deviation of elevation values. The Eq. 1.18, however, will only induce noise in the original DEM and the spatial dependence structure of the simulated DEM will not be the same as the original.

Rule 5 A robust way to reduce inaccuracies in terrain parameters is to average values from multiple realisations.
In order to preserve the same internal properties of the DEM (histogram and variogram), point simulation with kriging of the errors needs to be used to produce an equiprobable realisation of a DEM.

In order to produce a realisation of DEM with similar spatial dependence structure (i.e. similar *smoothness*), point simulation needs to be used [30]. It will produce a set of equiprobable realistic DEMs, each showing a similar histogram and variogram. Assuming gaussian spatial distribution of errors and for given $RMSE(z)$ and covariance function (C_0, C_1 and R), the realisation with same internal properties as the original DEM can be produced by simulating a point sample, inducing the error at point locations and then re-interpolating it over the whole area [1]. We suggest the following procedure for ILWIS:

(1) Randomly locate a set of points at locations α in the study area, so that the density of points corresponds to the original sampling density. In the case of contour data, average spacing between the contours (see Eq. 1.2) can be used to estimate the original sampling density:

$$\upsilon = \left[\frac{p}{L}\right]^2; \qquad \upsilon \in [0,1] \tag{1.19}$$

where p is the pixel size, and L is the average distance between the sampled points (contour data). Note that the sampling density is the key factor determining the smoothness of terrain[10].

(2) At these locations, assign a random error using the inverse normal probability function and given $RSME(z)$ (Fig. 1.3a and b):

$$\Delta z^{\alpha} = RMSE(z) \cdot \sqrt{-2 \cdot \ln(1-A)} \cdot \cos(2 \cdot \pi \cdot B); \qquad A, B \in [0,1) \tag{1.20}$$

(3) Interpolate the error at all grid nodes using the same variogram function as for the original DEM (Fig. 1.3c and d):

$$\Delta z_i^* = \sum w_i^{\alpha} \cdot \Delta z^{\alpha} \tag{1.21}$$

(4) Add the error surface (Fig. 1.3e) to the original DEM:

$$z_i^* = z_i + \Delta z_i^*; \qquad i = 1, ..., n \tag{1.22}$$

For each of the m simulated DEMs, terrain parameters are derived m times and then averaged per pixel:

[10] If the density of sampled points is high, it means that the terrain is more complex; if the density is low, the terrain is rather simple or smooth.

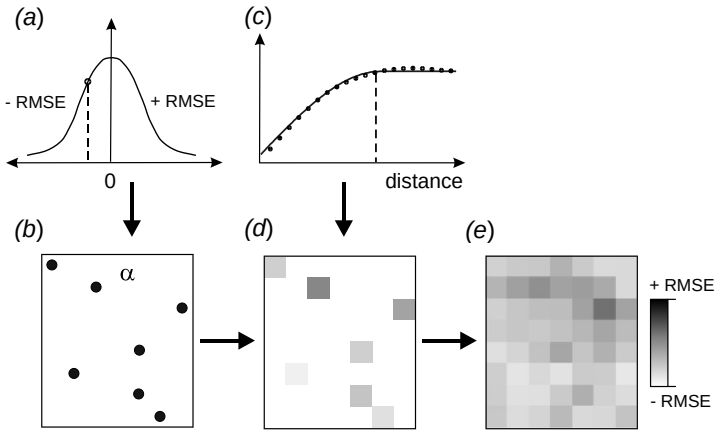

Figure 1.3: Schematic example of conditional simulation: simulated error (a) is assigned to random locations (b) and then interpolated using the variogram model of the DEM (c,d) to produce an error surface with the same internal properties as the input DEM (e).

$$\bar{\tau} = \frac{\sum_{j=1}^{m} \tau(z^{*j})}{m} \tag{1.23}$$

where $\bar{\tau}$ is the averaged map of a terrain parameter and $\tau(z^{*j})$ is the jth realisation of terrain parameter calculated from the simulated elevation map (z^*). More technical details on how to filter and improve original DEM and terrain parameters in ILWIS can be found on page 36.

1.3 Terrain parameters

The digital terrain parameters are commonly grouped in primary and secondary parameters [76]. We will use somewhat different classification, which primarily reflects the purpose of the analysis. Hence, three main groups will be described: a) morpohometric; b) hydrological and c) climatic parameters. The morpohometric terrain parameters describe the morphology of a surface, e.g. slope gradient, aspect and curvatures. Hydrological or flow-accumulation based terrain parameters describe potential flow of material, i.e. erosion hazard. Climatic terrain parameters are climatic variables adjusted to the factors of relief. In addition, we will introduce some new parameters, such as shape complexity index and potential drainage network density, and suggest a procedure to extract generic landforms (ridge, channel, plain, slope and pit).

1.3.1 Morphometric terrain parameters

The morphometric (or primary) terrain parameters are those that can be derived directly from the DEM using (local[11]) filter operations. Some early definition of morphometric parameters can be found even in the 19th century literature [23]. Young [81] gives a computer algorithm that uses matrix calculations. A standard reference for the formulas for calculation of primary attribute is the one by Zevenbergen and Thorne [83]. Somewhat different are Evens-Young method formulas, described by Pennock et al. [52]. The most recent overview is given by Shary et al. [61]. The morphometric terrain parameters can be grouped as follows:

- elevation change gradients: e.g. slope;
- orientation gradients: e.g. aspect, steepest downhill slope, viewshed;
- curvature gradients: e.g. horizontal or tangent curvature, vertical or profile curvature, mean curvature;

Rule 6 Slope shows the rate of change in elevation in x- and y-direction. Aspect gives azimuth angle of the sloping surface (orientation of central pixel). Negative plan curvature indicates concentration and positive divergence of flow; negative curvature indicates concave and positive convex profiles.

Plan curvature (PLANC) is curvature of corresponding normal section, which is tangential to a contour. Negative plan curvature indicates concentration and positive divergence of flow. Vertical or profile curvature (PROFC) is curvature of corresponding normal section, which is tangential to a flow-line. It is negative when the normal section concavity is directed up, and positive in the opposite case. Mean curvature (MEANC) is the average of normal section curvature. Negative MEANC values describe mean-concave landforms,

[11] Analysis within the first neighbouring pixels in e.g. 3×3 or 5×5 window environments.

while positive values refer to mean-convex ones. The TANGC, PROFC and MEANC are all expressed in 1/m or radians/m.

Z_{NB1} W_B	Z_{NB2} W_A	Z_{NB3} W_B
Z_{NB4} W_A		Z_{NB6} W_A
Z_{NB7} W_B	Z_{NB8} W_A	Z_{NB9} W_B

Figure 1.4: A common coding of adjacent cells. The black-square represents the cell being investigated.

In the case of the Evens-Young method [52], the terrain gradients are derived as:

$$G = \frac{df}{dx} = \frac{Z3 + Z6 + Z9 - Z1 - Z4 - Z7}{6 \cdot p} \tag{1.24}$$

$$H = \frac{df}{dy} = \frac{Z1 + Z2 + Z3 - Z7 - Z8 - Z9}{6 \cdot p} \tag{1.25}$$

$$D = \frac{d^2f}{dx^2} = \frac{Z1 + Z3 + Z4 + Z6 + Z7 + Z9 - 2 \cdot (Z2 + Z5 + Z8)}{3 \cdot p^2} \tag{1.26}$$

$$E = \frac{d^2f}{dx^2} = \frac{Z1 + Z2 + Z3 + Z7 + Z8 + Z9 - 2 \cdot (Z4 + Z5 + Z6)}{3 \cdot p^2} \tag{1.27}$$

$$F = \frac{d^2f}{dxdy} = \frac{Z3 + Z7 - Z1 - Z9}{4 \cdot p^2} \tag{1.28}$$

where G is the first derivative in x direction ($\frac{df}{dx}$), H is the first derivative in y direction ($\frac{df}{dy}$), D is the second derivative in x direction ($\frac{d^2f}{dx^2}$), E is the second derivative in y direction ($\frac{d^2f}{dx^2}$), F is the second derivative in diagonal direction ($\frac{d^2f}{dxdy}$), $Z5$ refers to the cell being investigated and p is the pixels size.

When calculating the second derivatives of elevation, it is advisable to smooth the elevation values ($Z5$) to get a more generalised picture of the terrain parameters. This is an empirical solution and its effect can differ from a dataset to a dataset. Evens and Cox [15] suggest the following equation:

$$Z5^+ = s \cdot \frac{Z1 + Z2 + Z3 + Z4 + Z6 + Z7 + Z8 + Z9}{9} + Z5 \cdot \left(1 - s \cdot \frac{8}{9}\right) \tag{1.29}$$

where $Z5^+$ is the smoothed value and s is the smoothing parameter.

All primary terrain parameters are then calculated from the five DEM gradients. The most common are slope (SLOPE), aspect (ASPECT), plan curvature (PLANC), profile curvature (PROFC) and mean curvature (MEANC) [61]:

$$SLOPE = \sqrt{H^2 + G^2} \tag{1.30}$$

$$ASPECT = \arctan\left(\frac{H}{G}\right) \tag{1.31}$$

$$PLANC = -\left(\frac{H^2 \cdot D - 2 \cdot G \cdot H \cdot F + G^2 \cdot E}{\left(G^2 + H^2\right)^{1.5}}\right) \tag{1.32}$$

$$PROFC = -\left(\frac{G^2 \cdot D + 2 \cdot G \cdot H \cdot F + H^2 \cdot E}{\left(G^2 + H^2\right) \cdot \left(1 + G^2 + H^2\right)^{1.5}}\right) \tag{1.33}$$

$$MEANC = -\left(\frac{\left(1 + H^2\right) \cdot D - 2 \cdot G \cdot H \cdot F + \left(1 + G^2\right) \cdot E}{2 \cdot \left(1 + G^2 + H^2\right)^{1.5}}\right) \tag{1.34}$$

Shape complexity index

In addition to the above-listed morphometric parameters, it might be also useful to describe the complexity of terrain features. This can be done by deriving the shape complexity index (SCI). SCI is commonly used to describe general geometry of shapes (polygons) in the sense of how simple (oval) some feature is (Fig. 1.5). It is derived as the perimeter-to-boundary ratio:

$$SCI = \frac{P}{2r\pi}; \qquad r = \sqrt{\frac{A}{\pi}} \tag{1.35}$$

where P is the perimeter of polygon, A is the area of polygon and r is the radius of circle with the same surface area [9]. A value of SCI close to 1 means that a polygon is rather compact and simple, while higher values describe narrow and long polygons (Fig. 1.5).

SCI can be derived by first slicing the DEM into equal elevation strata, then converting these strata to a polygon map (closed contours) and finally calculating the perimeter-to-boundary ratio (see user guide on 37 for more details). The SCI can be used to differentiate between the peaks and ridges, and pits and valleys: pits and peaks are more oval, while ridges and valleys are more longitudinal or dissected. Note that SCI does not have to be directly related to the roughness of terrain.

1.3.2 Hydrological terrain parameters

Hydrological or flow accumulation-based terrain parameters are typically used to describe flow of material over a gridded surface, i.e. quantify flow intensity, accumulation potential or erosion potential. In the most raster GIS applications flow accumulation algorithms are implemented by directing the flow into the lowest neighbouring cell. Imagining a tilted plane subdivided into square cells that is exposed to rain, one can determine the number

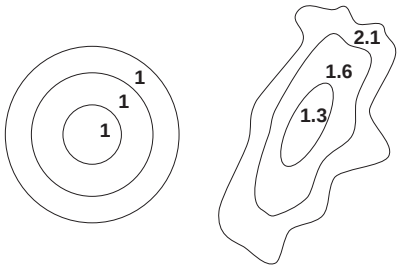

Figure 1.5: Comparison of the Shape complexity index values for perfectly oval shape (left) and different levels complexity (right).

of cells above each one cell that contribute water flowing through this cell (Fig. 1.6a). The lower the position of a cell is on this plane, the more area above will contribute water to it. Additionally, the form of the surface is important in directing the path of the accumulating flow. Peaks and ridges will tend to have diverging flow and low accumulation, whereas hollows or depressions will have a convergence of flow and a high accumulation of water. This hypothetical property of water accumulation is typically quantified by estimating the contributing area and local slope.

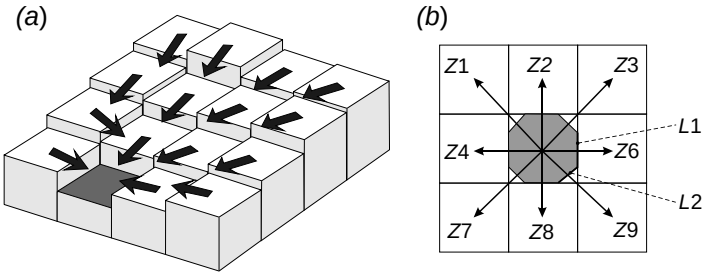

Figure 1.6: Schematic example of contributing cells at observed location (a) and effective contour lengths at cardinal and diagonal directions ($L1$ and $L2$) in a 3×3 window environment (b).

The tendency to accumulate water of a pixel with a low slope angle is greater than the one of a very steep pixel. Similarly it is evident that a pixel draining into many adjacent cells, i.e. over a great contour length, has a lower tendency to gather water than a pixel draining into only few adjacent cells. Commonly used parameter to describe this tendency at any point in the landscape is the *Compound Topographic Index* (CTI), also called *Topographic moisture index* or *wetness index*. It is defined as a ratio between the slope and catchment area:

$$CTI = \ln\left(\frac{A_f}{\tan\beta}\right) \tag{1.36}$$

where A_f is the specific catchment area draining through the point and β is the representative local slope angle. The natural logarithm re-scales the values to produce a normalized histogram. Note that, for the same contributing area, CTI is higher for pixels with lower slopes. This means that CTI primarily reflects the accumulation processes. To reflect the erosive power of the terrain, *Stream Power Index* (SPI) is used [49]:

$$SPI = A_f \cdot \tan\beta \tag{1.37}$$

Note that this index depicts areas of both high slopes and contributing areas. Another index often used to reflects the erosive power of the overland flow is the *Sediment Transport Index* (STI) [49]:

$$STI = \left(\frac{A_f}{22.13}\right)^{0.6} \cdot \left(\frac{\sin\beta}{0.0896}\right)^{1.3} \tag{1.38}$$

This empirical formula resembles the Universal Soil Loss Equation and can thus be used to depict locations of potential erosion risk. The formula for SPI can be adjusted using the plan, mean or profile curvature, e.g. plan curvature can be used to depict areas of ephemeral gullies [50]:

$$SPI_c = 0.2 \cdot [A_f \cdot (PLANC_{\max} - PLANC) \cdot \tan\beta]^{0.25} \tag{1.39}$$

This means that SPI is proportionally higher in the concave areas (concentration of flow). Note that all these parameters are purely empirical and formulas might different from literature to literature. Also note that for calculation of hydrological parameters (CTI, SPI and STI), the key issue is estimation of the specific catchment area and the slope gradient.

From the plan curvature (PLANC), we can also derive map of potential streams and ridges. The streams are highly concave and ridges highly convex areas. From the distance map to potential streams, we can derive the *potential drainage network density*. We suggest the following formula:

$$DDENS = \left(\frac{p}{p + d^*}\right)^{\varphi}; \qquad DDENS \in [0, 1] \tag{1.40}$$

where p is the pixel size, d^* is the distance to potential drainage network and φ is the adjustment factor[12].

Rule 7 Compound Topographic Index describes the tendency of terrain to accumulate water. Stream Power and Sediment Transport Indices describe tendency of flow and can be used to depict locations of potential erosion.

[12] Use 1.5 as the default value.

The multiple flow direction algorithm

The CTI, SPI and STI are commonly derived either using a single flow or multiple flow direction algorithms, and by considering either four or eight neighbours [84]. The single flow direction depicts only a main direction of flow (run-off), which may give rise to local inaccuracies. The multiple flow direction algorithm, on the other hand, distributes the upslope area among all possible directions and gives a more realistic picture of the water flow tendency. The multiple flow algorithm is described in detail by Quinn et al. [56]. It uses the slope-length maps to derive the drainage fraction out of each cell direction. Here, the main assumption is that the fraction of the area draining through each grid element is proportional to the slope angle into that cell. Thus, the drainage fraction ΔA_i out of a cell in a 3×3 window environment is equal to the slope-length fraction:

$$\Delta A_i = \frac{A_i}{\sum A_i} = \frac{\tan\beta_i \cdot L_i}{\sum(\tan\beta_i \cdot L_i)} = \frac{S_i}{\sum S_i}; \qquad i = 1,2,3,4,6,7,8,9 \tag{1.41}$$

where A_i is the upslope area in ith downhill direction, L_i is the contour length orthogonal to the ith direction and S_i is the slope-length. The slope-length maps are approximated in such a way that cardinal directions (cells 2, 4, 6 and 8) receive a slope length of $\frac{1}{2}$ grid size and diagonal directions (cells 1, 3, 7 and 9) receive a slope length of $\frac{\sqrt{2}}{4}$ grid size (Fig. 1.6b). The calculation of slope-lengths simplifies to:

$$S_{1,3,7,9} = \tan\beta \cdot L_2 = \frac{Z_5 - Z_{1,3,7,9}}{p \cdot \sqrt{2}} \cdot \frac{\sqrt{2}}{4} \cdot p = \frac{Z_5 - Z_{1,3,7,9}}{4} \tag{1.42}$$

$$S_{2,4,6,8} = \tan\beta \cdot L_1 = \frac{Z_5 - Z_{2,4,6,8}}{p} \cdot \frac{1}{2} \cdot p = \frac{Z_5 - Z_{2,4,6,8}}{2} \tag{1.43}$$

In a GIS, the drainage fractions can be propagated and summed to derive the total number of contributing cells. Each cell receives the value 1 plus the sum of the fractions of eight neighbours:

$$A_m = 1 + \sum_{j=1}^{m} \sum \Delta A_{ij}; \qquad i = 1,2,3,4,6,7,8,9 \tag{1.44}$$

where A_m is the cumulative drainage fraction from m neighbours. Note that this approach does not strictly preserve a water balance and should only be regarded as being an empirical approximation of water accumulation. Finally, the specific catchment area A_f can be derived as [56]:

$$A_f = \frac{A_m \cdot p^2}{\sum S_i} \cdot \tan\beta = \frac{A_m \cdot p^2}{\sum L_i} \tag{1.45}$$

where $\sum L$ is derived as the sum of lengths for draining pixels. Once the specific catchment area is determined, other indices such as CTI, STI and SPI can be estimated using the slope map.

1.3.3 Climatic terrain parameters

Calculation of climatic terrain variables, is in many cases much more complex than the calculation of the morphometric or hydrological variables. This is because, in general, a number of input parameters is required. In the case of modelling the direct diffuse and reflected solar insolation, number of operations can be fairly large [11]. In many cases, the computational formulations are vector based [8]. This makes it harder to implement in a raster-based GIS such as ILWIS.

In this lecture note, we will focus on only one climatic terrain parameter — *slope insolation* (SINS). This parameter can be used to describe the potential incoming solar radiation but also the wind exposure. Slope insolation is an approximation of solar radiation power expressed in percent. It depends on the Sun's position, i.e. azimuth and angle of sun from the horizon (Fig. 1.7). It can be compared to the calculation of shaded relief described by Horn [31]. The SINS is also derived using the first and second order derivatives [61]:

$$SINS = \frac{50 \cdot [1 + sign\,(\cos\alpha - \sin\alpha \cdot \{G \cdot \sin\beta + H \cdot \cos\beta\})] \cdot [\cos\alpha - \sin\alpha \cdot \{G \cdot \sin\beta + H \cdot \cos\beta\}]}{1 + G^2 + H^2} \tag{1.46}$$

$$sign(x) = \left\{ \begin{array}{ccc} 1 & \text{for} & x > 0 \\ 0 & \text{for} & x = 0 \\ -1 & \text{for} & x < 0 \end{array} \right\} \tag{1.47}$$

where G and H are the first order derivatives, α=90°-a, where a is the Sun vertical angle (ranges from 0 to 90°) from horizon and β is Sun azimuth counted from northern direction clockwise (ranges from 0 to 360°). Typically, light source in the 'standard cartographic position' is when the source of lights comes from the South (β=180°) and the Sun angle from horizon (α) is 45°.

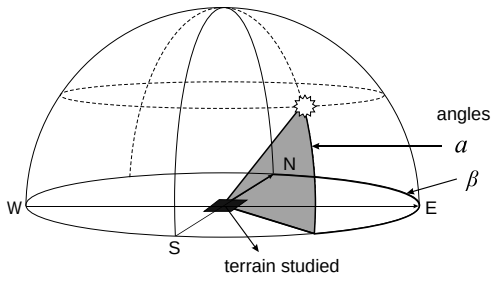

Figure 1.7: Insolation angles: Sun vertical angle (a) and Sun azimuth (β). Scheme by Shary et al. [61].

Note that the SINS accounts only for the direct exposition of a terrain towards a given point. In real cases, the cast shadow also needs to be accounted for. This means that,

although a terrain shows a direct exposition towards the source of light, one should also take into account that it could have been in a shadow of some neighbouring hills (Fig. 1.8). These areas can be detected using neighbourhood operation and masked with a 0 value.

Rule 8 Slope insolation is the solar radiation power from a point source, expressed in percent.

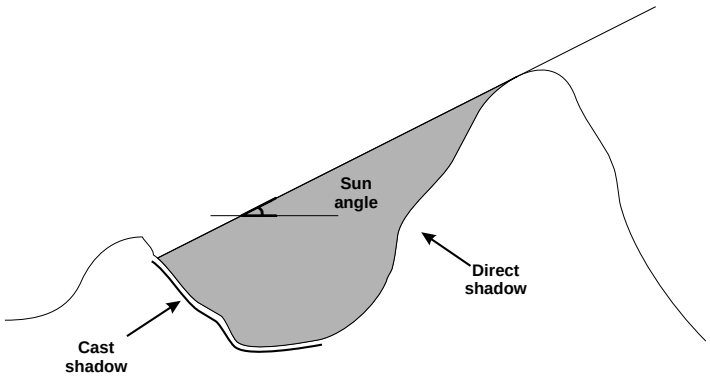

Figure 1.8: Schematic example of the cast shadow effect.

After we determined the relative solar insolation potential, we can also map the temperatures by:

$$T = T_b - \frac{\Delta T \cdot (z - z_b)}{1000} + C \cdot \left(S - \frac{1}{S}\right) \cdot \left(1 - \frac{LAI}{LAI_{\max}}\right) \tag{1.48}$$

where z is elevation at grid location, z_b is the elevation of the reference climatic station, T_b is the temperature at the reference station, ΔT is the temperature gradient (e.g. 5.06℃ per 1000 m), C is an empirical constant (e.g. 1{textcelsius), S is the short-wave radiation ratio, LAI is the leaf area index at the grid cell and $LAI_{\max}$ is the maximum leaf area index. In this case, LAI can be neglected and S can be estimated from SINS:

$$S = \frac{SINS}{SINS_0} \tag{1.49}$$

where $SINS_0$ is the slope insolation on horizontal site (slope=0).

1.3.4 Generic morphometric features

Classification and description of geomorphic features is a study by itself. The most geomorphological classification systems are based on photo-interpretation and geological characterisation of an area. In the case of DTA, it is possible to extract some generic morphometric features from the DEM in a semi-automated or auto-mated manner. Some early algorithms to extract peaks, pits, ridges and ravines from the contour map are given by Kweon and Kanade [37]. Woo [79] recognizes six generic terrain features: pits, peaks, channels, ridges, passes and planes. Their automated extraction is possible in LANDSERF by setting up tolerance values for each class.

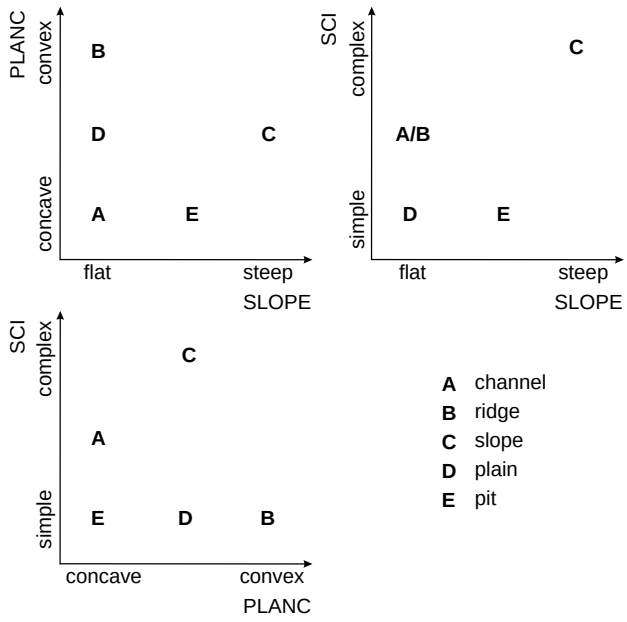

Figure 1.9: Definition of generic landforms using slope (SLOPE), plan curvature (PLANC) and shape complexity index (SCI).

We recommend somewhat modified list of generic landforms[13] (see Table 1.2). These are derived using three terrain parameters: SLOPE, PLANC and SCI. Note that the definition of classes and class centres (Fig. 1.9) is arbitrary and might require modifications for different study areas. However, these five landform shapes can be used to represent the most common morphometric features.

Because the definition of the generic landforms is difficult and there will always be some overlap between the classes (e.g. between pit and valley bottom), a continuous classification system such as fuzzy k-means is recommended [6]. In fact, the membership grades for each

[13]This is an arbitrary definition.

Table 1.2: Generic landforms, their description and relation with terrain parameters.

Landform	Description	SLOPE	PLANC	SCI
Stream channel (Valley bottom)	Locations of water accumulation and transition; high number of upstream elements and concave shapes	min	min	avg
Ridge (Peak)	Locations of water run-off; lowest upstream contributing area and convex shapes	min	max	min
Slope	Sloping part with generally higher shape complexity	max	avg	max
Plain (Terrace)	Flat areas of low relief and low shape complexity	min	avg	min
Pit	Conical concave landform	avg	min	min

generic landform can be termed: *channel-ness*, *ridge-ness*, *slope-ness*, *terrace-ness* and *pit-ness*. These attribute memberships can be treated as a special type of terrain parameters also.

Chapter 2

User guide

2.1 The study area

In the following sections filtering of a DEM and calculation of terrain parameters is explained in chronological order. We used a small dataset "Baranja hill", which has been mapped extensively over the years (Hengl and Rossiter, 2003). The study area is located in Eastern Croatia (centred on 45°47'40" N, 18°41'27" E). The main geomorphic facets are hill summits and shoulders, eroded slopes of small vales, vale bottoms, a large abandoned river channel, and high and low river terraces (Fig. 2.8). Contour lines were extracted from the 1:50 K topo-map (Fig. 2.8b), with the contour interval of 10 m and supplementary 5 m contours in areas of low relief. The total area is 13.69 km^2 and elevations range from 80 to 240 m. There were 127.6 km of contour lines in total, which means that the average spacing between the contours is 107 m and the pixel size should be at least 50 meters to present all mapped changes in relief (Eq. 1.2). Because the spacing between the contours is much narrower in the hill than in the plain, we finally decided to use a grid resolution of 25 m. The Baranja hill dataset[1] consists of:

Baranja hill dataset	
Spatial object name	Description
`Contours`	Segment map representing contours (90-240 m)
`W_bodies`	Raster map of water-bodies (`stream`, `lake` and `channel`)
`Geoform`	Polygon map of the main geoforms (landform facets)
`AP`	Aerial (ortho-rectified) photo of the study area (pixsize=5 m)

The bounding coordinates (X, Y at centre of pixels) are: 6551897.5, 5070575; 6555547.5, 5074275, according to the Croatian coordinate system (Zone 6). The map consists of 149 rows by 147 columns. This corresponds to the size of a single 1:20 K aerial photo. The aerial photo can be used to overlay the derived DTA vector products and evaluate their quality.

The contour lines were interpolated using the linear interpolator in ILWIS. The algorithm is described in more detail by Gorte and Koolhoven [25]. The contour interval is 20 m in hill and 5 m in the plain, hence we used the $RMSE(z)$ of 5 m in the hilland and 1.25 m in the plain. The unfiltered DEM was used to georeference the aerial photo (AP), which was then resampled to produce the ortho-photo of the area [59]. The grid resolution of AP is 5 m.

We assume the student is familiar with ILWIS 3.0. Detailed explanation of GIS operations and ILWIS commands can be found in the ILWIS help documentation or user's guides[2]. In order to speed-up the calculation of terrain parameters it is advisable to create ILWIS scripts using the ILWIS language. If you need more details on how to create and run a script, we advise you to read ILWIS 3.0 Academic user's guide, §12. The ILWIS script consists of set of commands that can be used with up to nine script parameters. These can be either spatial objects, values or textual strings. The script in principle consists of two parts: definition of script parameters and list of commands. Sign "//" is used to exclude to insert comments and explanation of formulas.

[1] Download zipped files from `http://www.itc.nl/personal/shrestha/DTA/`, 705 KB

[2] Both available on-line at `http://www.itc.nl/ilwis/`

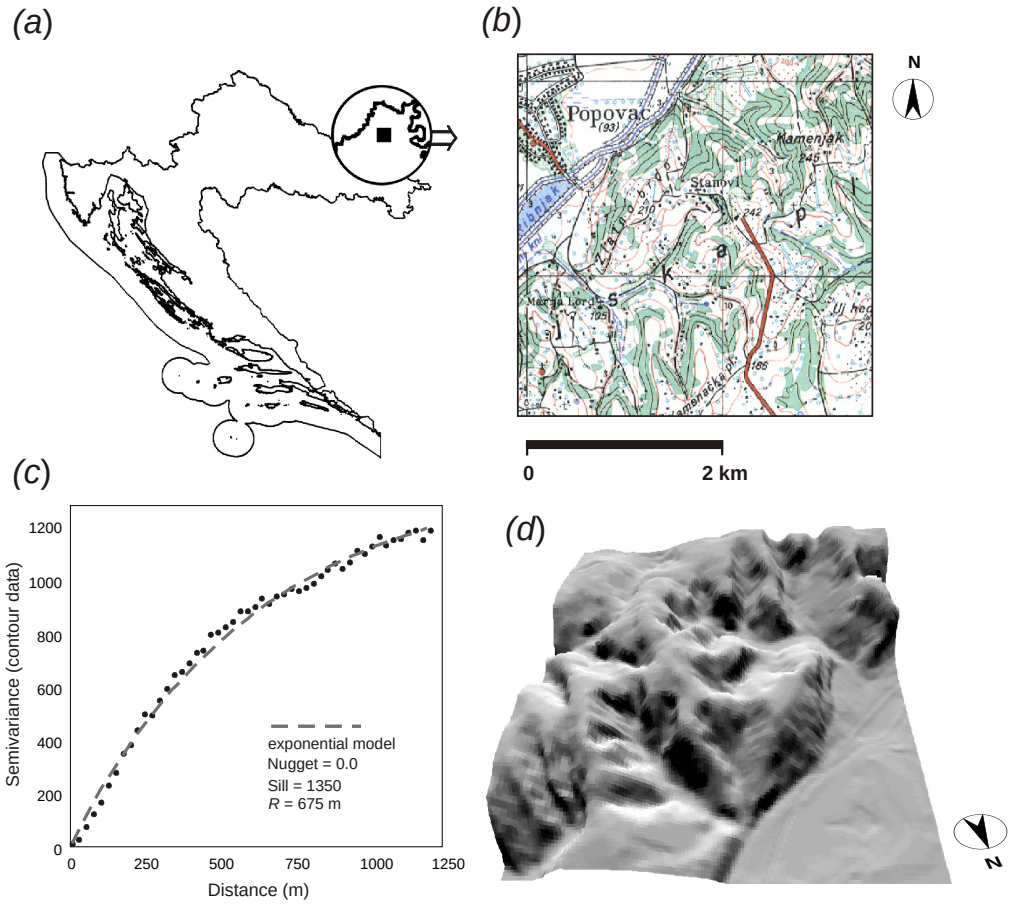

Figure 2.1: Study area *Baranja hill*: (a) location in Eastern part of Croatia; (b) 1:50 K topo-map used to derive contour lines; (c) variogram modelling of the contour data and (d) perspective view.

2.2 Pre-processing of DEM

Prior to derivation of terrain parameters, we need to improve the plausibility of the DEM as explained in section 1.2.5. There are several approaches to improve the geomorphic resemblance of the DEM and reduce the artefacts in the terrain parameters. Here, we suggest three steps, which are based on filtering and neighbourhood GIS operations with iterations and can be used more or less universally in any area. Consequently, there are four levels of DEM:

- (DEM_L0) the unfiltered (original) DEM - derived from the contour data only;
- (DEM_L1) terrace-free DEM - padi terraces are replaced by digitising ridges, peaks and sinks or by using automated extraction of medial axes;
- (DEM_L2) smoothed DEM - filtered for the outliers;
- (DEM_L3) streams-adjusted DEM - elevation adjusted for the streams and water bodies;

The final product of the filtering (DEM_L3) was further on used to derive terrain parameters. First, the padi terraces need to be detected and masked from the original DEM:

```
DEM_TER=iff((nbcnt(DEM#=DEM)>7), ?, DEM)
```

This will detect areas where more than seven neighbouring pixels have exactly the same elevation. Now the medial axes can be detected using the distance operation with the rasterized map of contours [55]:

```
CONT_dist=MapDistance(ContoursRasterized.mpr)

MED_AXES{dom=Bool.dom}=iff((nbcnt(CONT_dist>CONT_dist#)>4) AND
(isundef(DEM_TER)), 1, 0)
```

Here the map MED_AXES shows detected valley bottoms and ridges, where value "1" or "True" represents the possible medial axes (Fig. 2.2b). We can attach to these areas some small constant value and then re-interpolate the DEM map. Before we do that, we need to detect which of these medial axes are ridges and which valley bottoms, i.e. which are convex and which concave areas. This can be done by two ways:

- using the neighbourhood operation[3]:
  ```
  FORM_tmp{dom=Bool.dom}=iff(DEM>nbavg[2,4,6,8](DEM_TER#), 1,
  iff(DEM_TER<nbavg[2,4,6,8](DEM_TER#), 0, ?))
  ```

- an alternative is to derive the mean curvature from the unfiltered DEM and then classify it using:
  ```
  FORM_tmp{dom=Bool.dom}=iff(MEANC>0, 1, iff(MEANC<0, 0, ?))
  ```

The temporary shape map (FORM_tmp) can be extrapolated using the map iterations to fill the undefined pixels:

```
FORM_ext=MapIter(FORM_tmp.mpr, iff(isundef(FORM_tmp), nbprd(FORM_tmp#), FORM_tmp))

FORM=MapIter(FORM_ext.mpr, nbprd(FORM_ext#), 5)
```

The last command is used to smooth the FORM map and reduce possible artefacts (we recommend at least five iterations). The derived map of the general terrain shape can be

[3]The convex terrains (ridges) receive value "1" or "True" and concave terrains (valleys) value "0" or "False". The padi terrace areas will receive undefined value.

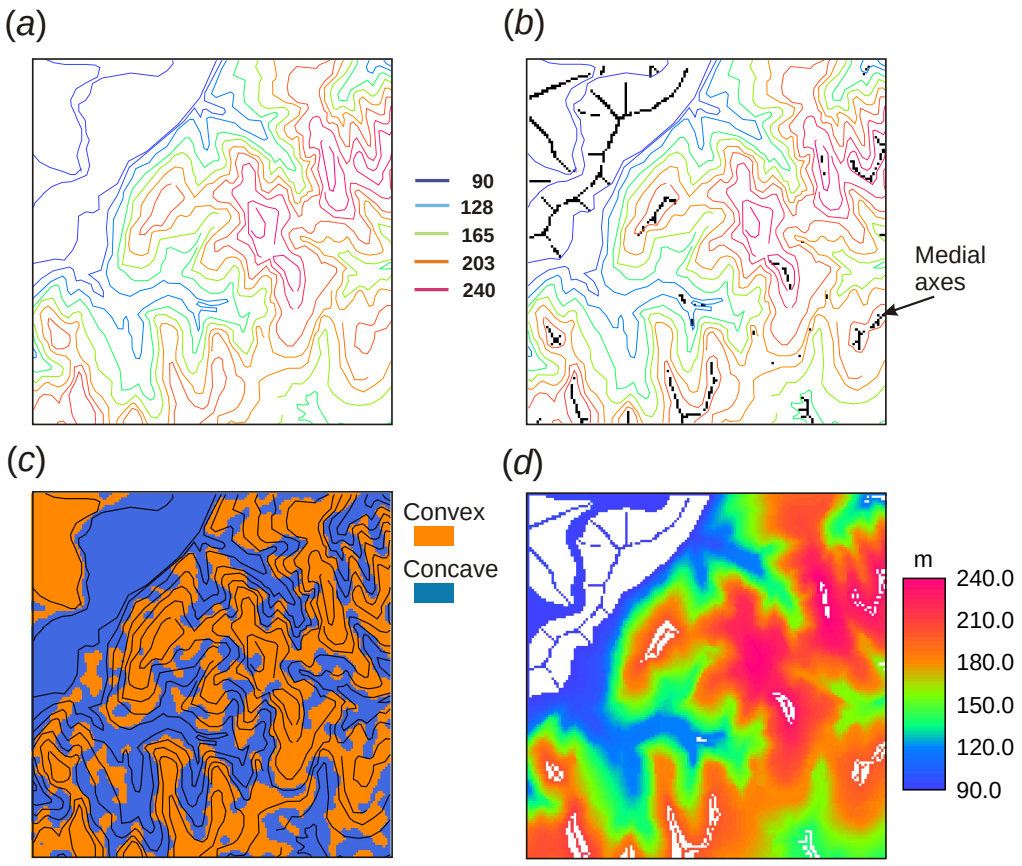

Figure 2.2: Addition of medial axes: (a) original (bulk) contour data; (b) detected medial axes in problematic areas (padi terraces); (c) extrapolated shape of the terrain and (d) temporary terrace-free map prior to interpolation of the remaining undefined pixels.

seen in Fig. 2.2c. This can be very important in the more rugged terrains. Finally a constant value (*RMSE*) is attached to the medial axes (Fig. 2.2d) and the remaining undefined pixels are interpolated using kriging from raster operation in ILWIS:

```
DEM_tmp=iff(MED_AXES=True, iff(FORM=True, DEM+RMSE,
iff(FORM=False, DEM-RMSE, DEM_TER)), DEM_TER)

DEM_L1.mpr{dom=value.dom;vr=0.0:5000.0:0.1}=MapKrigingFromRaster(DEM_tmp,
SemiVarModel, LimDist, Distance Unit, 1|0, min, max)
```

In this case you can use the following parameters: `SemiVarModel=Exponential(0.0, 1350, 675), LimDist=40, Distance Unit=p, 0, min=1, max=10`. The fitted variogram of the contour data is shown in Fig. 2.2c. Note that it is advisable to use a map of $RMSE(z)$ instead of the constant value, because in this case, the contour interval differs in plain and in hill region. In this case a more accurate `RMSE` map was produced using the Eq. 1.3 and slope map:

```
RMSE_z=iff(DEM<100, 1.25+10*SLOPE/100, 5+10*SLOPE/100)
```

After the filtering of padi terraces, the outliers can be reduced using the probability of exceeding a value estimated from the neighbours. First predict the central value from the neighbours using the kriging weights calculated in a 3×3 window:

```
Z_PRED=DEM#[1]*-0.003+DEM#[2]*0.253+DEM#[3]*-0.003+DEM#[4]*0.253+DEM#[6]*0.253
+DEM#[7]*-0.003+DEM#[8]*0.253+DEM#[9]*-0.003
```

where $w_{\mathrm{A}} = 0.253$ and $w_{\mathrm{B}} = -0.003$ are the kriging weights, calculated for the given covariance function. Then, calculate the difference between the original and predicted elevation:

```
Z_DIF=DEM-Z_PRED
```

This difference should follow a normal distribution. In this case, the overall average difference is 0 and standard deviation is 1.28 m. The differences can now be standardize using the overall standard deviation:

```
Z_DIFS{dom=value.dom;vr=-50.000:50.000:0.001}=Z_DIF/S_DIF
```

Note that we could have also used the $RMSE(z)$ to standardize the differences. The `Z_DIFS` is the t-value, which can be converted to the normal probability using:

```
Z_PROB{dom=value.dom;vr=0.000:1.000:0.001}= (1/sqrt(PI2))*exp(-sq(Z_DIFS)/2)/0.4
```

Now use this probability as the weight function to derive the smoothed DEM:

```
DEM_L2{dom=value.dom;vr=0.0:5000.0:0.1}=Z_PROB*DEM+(1-Z_PROB)*Z_PRED
```

where `Z_PROB` is the normal probability to find a certain value[4], `Z_PRED` is the map of elevations predicted from the neighbours. In the last step, the existing information on water bodies (`W_bodies`) is used to adjust the DEM (see Eq. 1.19):

```
W_dist=MapDistance(W_bodies)
```

[4]In this case we work with the Gaussian function and then divide it with the maximum value (0.4). This is done because ILWIS can not provide inverse normal distribution calculation.

```
DEM_L3{dom=value.dom;vr=0.0:5000.0:0.1}=iff(isundef(W_bodies),
DEM-(pixsize(DEM)/(pixsize(DEM)+W_dist))^1.5*2.5,DEM-2.5)
```

where H is the maximum elevation difference, `W_dist` is the distance map from the water bodies and φ=1.5 is the adjustment factor and For H=2.5 is the empirical value. Here we used half the contour interval (2.5 m) as the maximum difference.

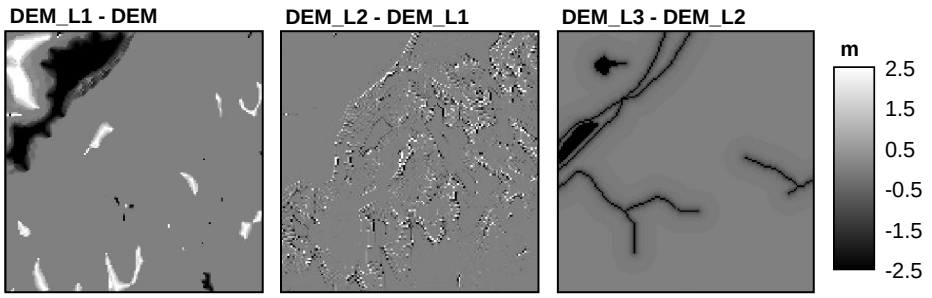

Figure 2.3: Automated DEM filtering in three steps — change in elevation values.

The filtering levels and consequent change in the DEM can be seen in Fig. 2.3. Note that these steps do not guarantee that 100% of artefacts will be removed. It is advisable to check the percentage of artefacts and, if needed, digitise extra contours, use extra auxiliary information or use higher number of iterations. Note that the changes to the DEM that resulted from this filtering are relatively small, i.e. within half the contour interval. It cannot be excluded, however, that also a small number of real features such as small lakes and depressions that can occur naturally were corrected away.

2.3 Deriving morphometric parameters

Calculation of terrain parameters can be easily automated using the ILWIS scripts. Here we implemented the Evens-Young method formulas, explained in detail by Shary et al. [61]. The input parameters and ILWIS script can be seen in Table 2.1, on page 2.1. Note that PLANC, PROFC and MEANC calculated using Eqs. 1.31 to 1.34 might show local artefacts, unrealistic values or can be undefined. In order to get a more general (natural) picture of curvatures, it is suggested to smooth the second derivatives ($\frac{d^2f}{dx^2}$, $\frac{d^2f}{dx^2}$, $\frac{d^2f}{dxdy}$) by using filtering operation. The second problem is the undefined pixels, which are either due to division by zero or these are values outside a feasible range. The undefined pixels are replaced by iteratively taking the predominant value from the neighbours.

2.3.1 Reducing errors by error propagation

Even after these two filtering steps, the terrain parameters might not reflect the terrain shape as accurately as we aspect. A way to improve the appearance of the terrain parameters is to run several realizations (simulations) with induced error and then average the terrain parameters. The procedure is explained in section 1.2.6. First the sampling density is estimated from the average spacing of contours (107 m) and total area (13.69 km^2) using Eq. 1.19. This gives value of 0.06. DEM is then simulated using:

```
RND_n=DEM*0+rnd()

DELTA_p=iff(RND_n>0.06, ?, RMSE_z*sqrt(-2*ln(1-rnd()))*cos(2*PI*rnd()))

DELTA.mpr=MapKrigingFromRaster(DELTA_p, SemiVarModel, LimDist, Distance Unit,
1|0, min, max)

DEM_csim01.mpr= DEM + DELTA
```

where `RND_n` is a temporary map of random values from 0 to 1, `DELTA_p` is a randomized point map with simulated error, `RMSE_z` is the map of estimated errors (Eq. 1.3) and `DELTA` is the simulated error surface with the same spatial correlation structure (Fig. 2.4). Note that the error surface is smooth, which is somewhat different from the conditional simulations [30, see also `http://www.geog.ucsb.edu/ karen/`], where the simulated DEM might show noisy patter[5].

Elevation is simulated m times[6] and for each simulated DEM a terrain parameter is calculated using a script (Table 2.1 on page 2.1). The average terrain parameter is then derived using (Eq. 1.23).

As a result of reduction of errors by propagation, the terrain parameters will be smoother, with much less artefacts and more natural appearance. The Fig. 2.5 shows, for example, difference between PLANC calculated using the original DEM and 20 realisations. Note that the right image shows connected, smoother features; also note that the artefacts in the plain region will disappear from the PLANC map after several realisations.

Parameters for the `TP_MORPH` script			
Parameter	Spatial object name	Type	Default object
%1	Digital elevation map	Raster map	`DEM_L3.mpr`
%2	Smoothing parameter[7] (s)	Value	0.5

[5] We believe that this is only introduction of artefacts that do not reflect true topography — even simulated topography needs to be as smooth as the input DEM.

[6] We recommend at least 50 realisations, although improved results will be visible even after 20 realisations.

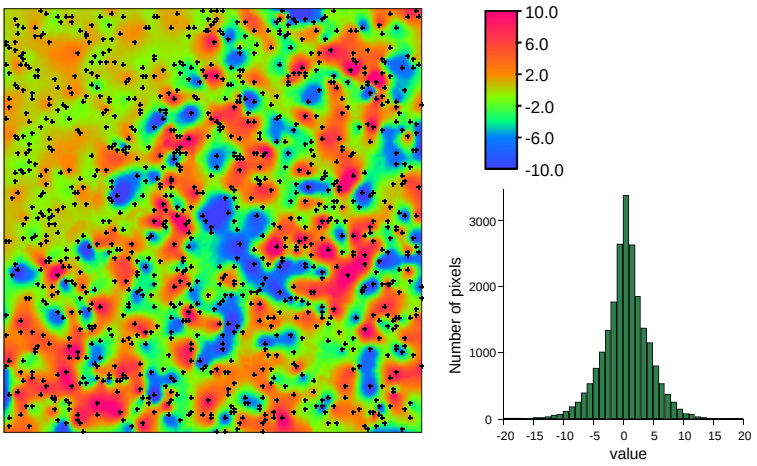

Figure 2.4: Simulated error surface (`DELTA`) with randomly located sampling points and map histogram. Note that the *RMSE* is much smaller in plain region.

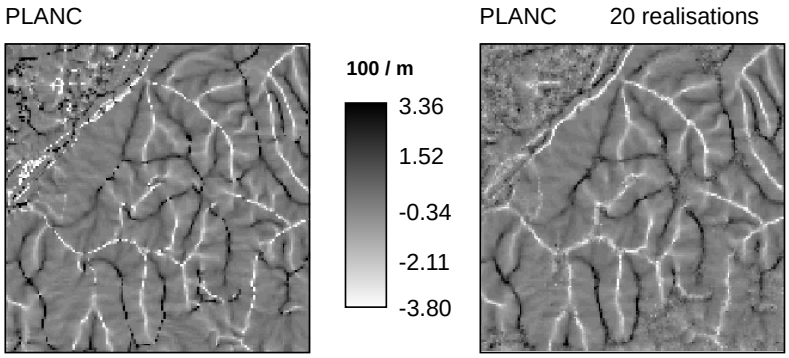

Figure 2.5: Comparison of PLANC calculated using the original DEM and 20 realisations.

The list of morphometric terrain parameters of the study area can be seen in Fig. 2.6.

2.3.2 Shape complexity index

The SCI is derived as follows. First the DEM map is sliced using an equal interval, e.g. 5 m (you can derive W using the Eq. 1.6, in this case N=21903, $RMSE$(DEM)=43.81 m, which

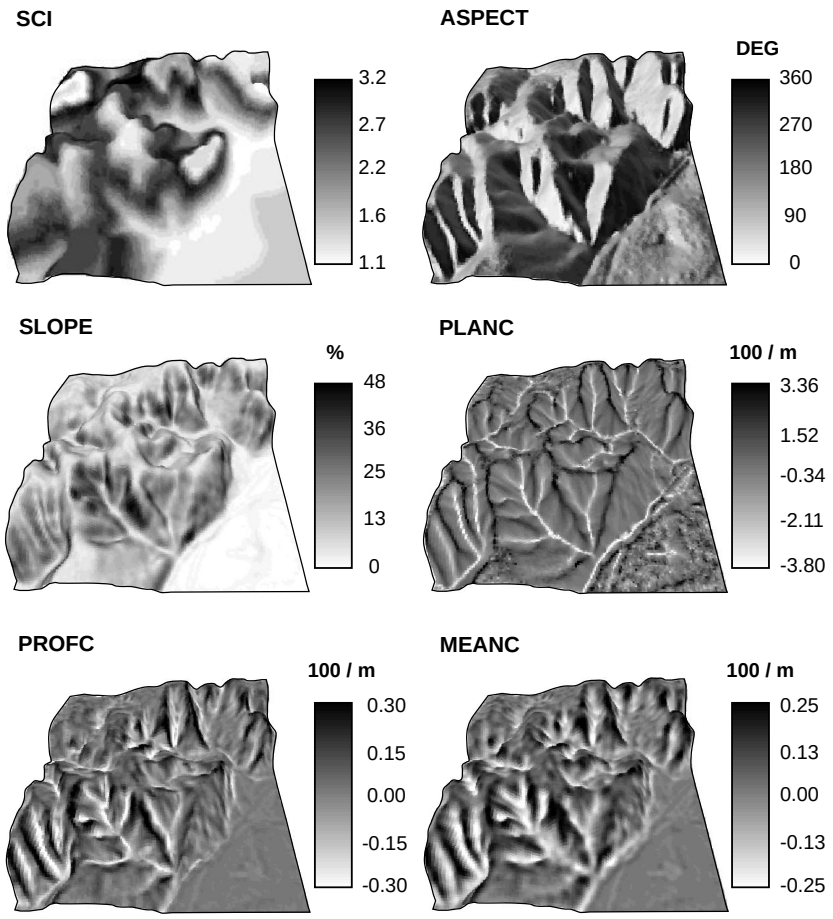

Figure 2.6: SCI (Shape Complexity Index) and derived morphometric terrain parameters: ASPECT (0–360°), SLOPE (slope in %), PLANC (plan curvature), PROFC (vertical curvature) and MEANC (mean curvature), all derived using 20 realisations.

gives optimal bin width of W=5.5 m). For example, for the contour interval 90 and higher, the DEM is sliced using:

```
class_090dom=DEM_5m=iff(DEM<90,?,"90")
```

where `DEM_5m` is the group domain with elevation classes 85, 90, 95 etc. This gives a stratified map, which can be polygonized using:

```
pol_090.mpa=PolygonMapFromRas(class_090,8,smooth)
```

```
pol_090ID.mpa=PolygonMapNumbering(pol_090.mpa,,ID)
```

where pol_090ID is a polygon map with each polygon having an unique ID, so that SCI can be derived locally. The SCI is then calculated using:

```
pol_090ID.hsa=TableHistogramPol(pol_090ID.mpa)

calc pol_090ID.hsa

tabcalc pol_090ID.tbt Perimeter=ColumnJoin(pol_090ID.hsa,Perimeter)

tabcalc pol_090ID.tbt SCI=Perimeter/(2*sqrt(Area/PI)*PI)

SCI090.mpa=PolygonMapAttribute(pol_090ID,SCI)

SCI090.mpr=MapRasterizePolygon(SCI090,georef)
```

The SCI needs to be calculated for all elevation classes, which gives a large number of maps[8] and can be very computationally demanding. The maps-slices are then glued to produce an overall map of SCI:

```
SCI.mpr = MapGlue(SCI080,SCI085,SCI090, ...)
```

Due to the discretisation level of elevation classes (in this case 5 m), the final SCI map might show abrupt change of values. Therefore, it is advisable to smooth the overall SCI (average filter) to produce a more general picture.

2.4 Deriving hydrological terrain parameters

The generation of specific catchment area and slope length maps can be automated in ILWIS using the multiple flow direction algorithm, as explained in subsection 1.3.2 on page 23. The calculation consists of four steps:

- Generate the slope-lengths for each diagonal and cardinal direction (8 maps) and their sum;
- Generate the drainage fraction out of cell for each direction;
- Generate drainage fraction into each cell for each direction as a fraction of the contributing cell (Fig. 2.7);
- Propagate the total number of contributing cells using n iterations with start map consisting of 1's (Fig. 2.8).

[8] In this case W=5 m, which gives about 30 maps-slices.

A script to derive the catchment area can be seen in Table 2.2, on page 2.2. Note that the `CATCH_tmp` map is iteratively filtered for undefined pixels[9] by taking the predominant value from the surrounding pixels until all zero slopes are replaced. This is especially important because in ILWIS the undefined pixels will otherwise propagate. This filtering has the effect of creating pools of high CTI in the plain, which is in general realistic.

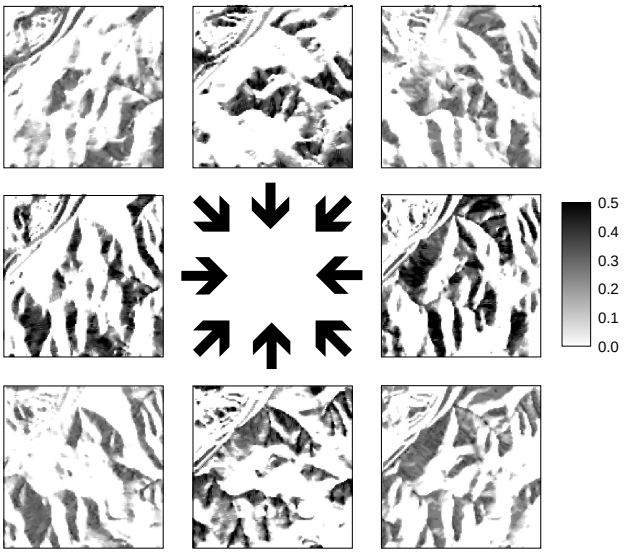

Figure 2.7: Drainage fraction elements in each direction — ΔA_i see Eq. 1.41.

Parameters for the `FLOW` script			
Parameter	Spatial object name	Type	Default object
%1	Digital elevation map	Raster map	`DEM_L3.mpr`
%2	Study area (? for excluded areas)	Raster map	`DEM_L3.mpr`
%3	Number of iterations[10]	Value	20–150

[9]Division by zero — locations where `LSUM`=0.

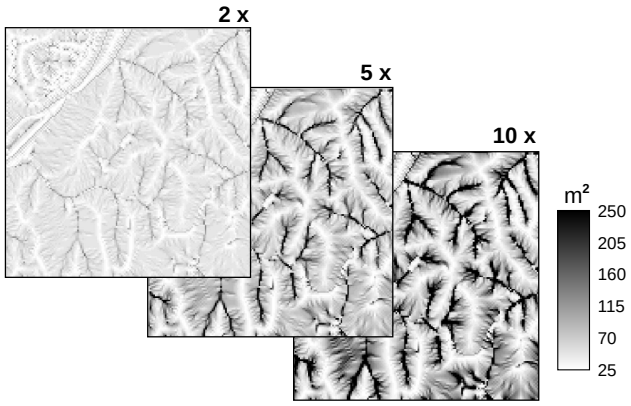

Figure 2.8: Specific catchment area after 2, 5 and 10 iterations.

Each new iteration will propagate flow by a distance equal to the pixel size or the diagonal pixel size. This should be ideally done until only very few downstream pixels are changed with any new calculation, which can be checked by evaluating a difference map of accumulation after n and after $n + 1$ iterations. In this case we used only 20 iterations for flow accumulation. This small number of iterations was sufficient, because remaining changes with further iteration were only in stream bottoms, which already had a high CTI relative to other landscape positions. Note that the propagation of the drainage fraction is a time consuming task. A 149×147 pixel map with 50 iterations takes about 10 minutes to calculate in ILWIS 3.11 on a Pentium III 760MHz Computer.

After the catchment area has been derived, wetness index (CTI), Stream power index (SPI) and Sediment transport index (STI) can be derived using:

```
CTI{dom=value.dom;vr=0.00:5000.00:0.01}=ln(CATCH/SLOPE*100)

SPI{dom=value.dom;vr=0.0:500000.0:0.1}=CATCH*SLOPE/100

STI{dom=value.dom;vr=0.0:500000.0:0.1}=(CATCH/22.13)^0.6*
(sin(ATAN(SLOPE/100)))/0.0896)^1.3
```

Raster stream networks can be generated by distinguishing pixels that have are fairly concave or convex, i.e. higher or lower than a set threshold value. Stream and ridges can be detected by:

```
streams_pixdom=Bool=iff(PLANC<-1.5, True, False)

ridges_pixdom=Bool=iff(PLANC>1.5, True, False)
```

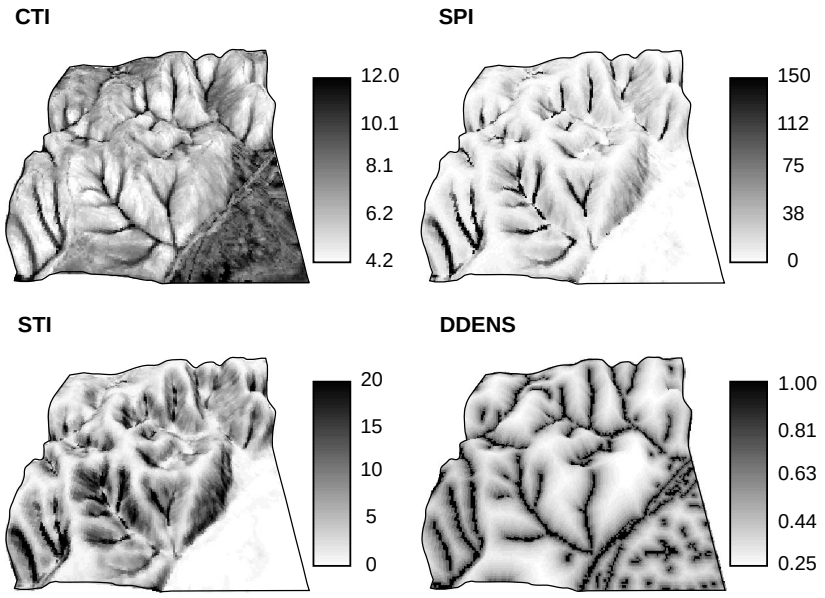

Figure 2.9: Hydrological terrain parameters: (a) Compound Topographic Index (CTI); (b) Stream Power Index (SPI); (c) Stream Transport Index (STI) and (d) potential drainage network density (DDENS).

It is advisable to propagate the remaining areas to surrounding locations by using the DEM map:

```
STREAMS_tmp.mpr=MapIterProp(streams_pix.mpr, iff((nbcnt(DEM#>DEM)>5),
nbmax(streams_pix#), streams_pix))

RIDGES_tmp.mpr=MapIterProp(ridges_pix.mpr, iff((nbcnt(DEM#<DEM)>5),
nbmax(ridges_pix#), ridges_pix))
```

The temporary maps can show number of single pixel streams/ridges, which need to be filter using the neighborhood operation:

```
STREAMS{dom=value.dom;vr=0:1:1}=iff(nbcnt(STREAMS_tmp#=0)>7, 0, STREAMS_tmp)

RIDGES{dom=value.dom;vr=0:1:1}=iff(nbcnt(STREAMS_tmp#=0)>7, 0, STREAMS_tmp)
```

The map of potential streams (Fig. 2.10 can be used to derive a buffer map, which is then used to derive the potential drainage density (Eq. 1.40):

```
DDENS{dom=value.dom;vr=0.000:1.000:0.001}=(pixsize(S_dist)/
(S_dist+pixsize(S_dist)))^1.2
```

where `S_dist` is the buffer map for potential streams.

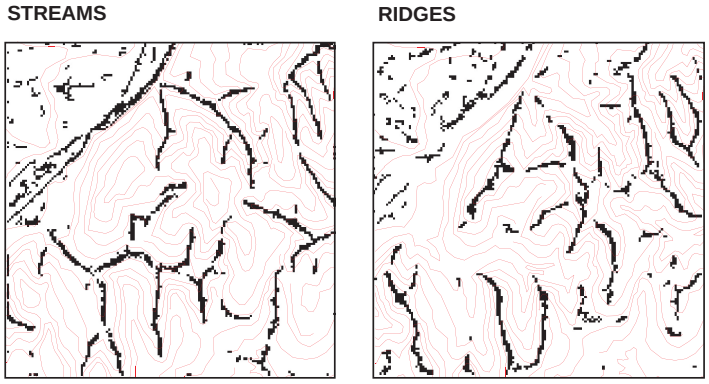

Figure 2.10: Automatically detected potential streams and ridges.

2.5 Deriving climatic terrain parameters

The key parameter that explains relative potential to receive direct solar insolation is the slope insolation (SINS). Calculation of SINS in ILWIS is straightforward:

```
SINS.mpr{dom=value.dom;vr=0.0:100.0:0.1}=50*(1+iff((cos(degrad(90-a))
-sin(degrad(90-a))*(dx*sin(degrad(b))+dy*cos(degrad(b))))>0, 1,iff
((cos(degrad(90-a))-sin(degrad(90-a))*(dx*sin(degrad(b))+dy*cos(degrad(b))))
<0,-1,0)))*(cos(degrad(90-a))-sin(degrad(90-a))*(dx*sin(degrad(b))
+dy*cos(degrad(b))))/(1+dx^2+dy^2)
```

where `dx` and `dy` are the first derivatives of elevation in x and y direction, a is the a and b is the β in Eq. 1.46. Note that the ILWIS command is somewhat longer because the sign (Eq. 1.47) needs to be checked.

The cast-shadow and direct shadow areas can be detected by iteratively inspecting the local slope angle. If the local angle is higher than the sun angle, the input DEM is iteratively filled until there is no location with an angle higher than the sun angle. This can be done only for each of the eight directions. For example, if the sun position (azimuth) is at 180°, the shadows can be detected as:

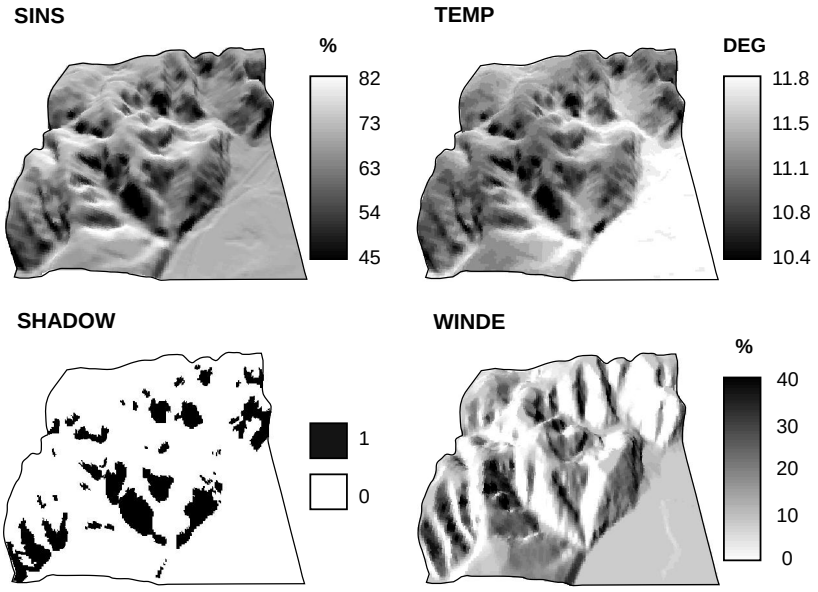

Figure 2.11: Climatic terrain parameters: slope insolation (SINS) with sun angle at 45˚ and azimuth at 180˚; mean annual temperature (TEMP) adjusted for the elevation and radiation ratio; map of shadows if sun angle is at 15˚ and wind exposition potential (WINDE) to West-East directed winds.

```
DEM_SH=MapIter(DEM.mpr, iff( ((DEM#[8]-DEM)/pixsize(DEM))>0.5 or
((DEM-DEM#[2])/pixsize(DEM))>0.5, DEM#[8]-pixsize(DEM)*0.5, DEM))
```

where `DEM_SH` is the DEM is without any slope higher than the sun angle (45˚). The shadow areas can no be simply depicted as the areas where a change occured:

```
SHADOW{dom=value.dom;vr=0.0:1.0:0.1}=iff(DEM_SH=DEM,1,0)
```

which can be used to adjust `SINS` map for direct and cast shadows (Fig. 2.11):

```
SINS_SH=SHADOW*SINS
```

From the SINS map and temperature data from the climatic station, we can also map the mean annual temperature of the area using the Eq. 1.48:

```
TEMP{dom=value.dom;vr=-10.0:30.0:0.1}=10.8-5.06*(DEM-90)/1000+
(SINS/63-1/SINS*63)
```

In this case we used the referent station at elevation of 90 m (z_b). The mean annual tem-

perature was 10.8°C (T_b) and $SINS_0$=63. Note that because the range of elevations is low (90-240 m), the dominant factor controlling the local temperatures is the SINS (Fig. 2.11).

2.6 Extraction of generic landforms

Generic landforms - channel, ridge, plain (terrace), slope and pit can be derived using the supervised fuzzy k-means classification. In this case, the input maps needed are the SLOPE, PLANC and SCI maps, fuzzy exponent and a table with definition of class centres (see Table 2.3 on page 2.3).

Parameters for the GLF_fkm script			
Parameter	Spatial object name	Type	Default object
%1	Class centres	Table map	LF_class.tbt
%2	Fuzzy exponent	Value	1.5
%3	Landform classes	Domain	landforms.dom
%4	Slope	Raster map	SLOPE
%5	Plan curvature	Raster map	PLANC
%6	Shape complexity index	Raster map	SCI

In this case, the LF_class.tbt table with the definition of classes looks like this:

	SLOPE	PLANC	SCI	SLOPE_STD	PLANC_STD	SCI_STD
channel	5	-2	1.5	5	0.5	0.5
pit	5	-2	1	5	0.5	0.5
plain	0	0	1	5	0.5	0.5
ridge	5	2	1.5	5	0.5	0.5
slope	25	0	3	5	0.5	0.5

Note that we have approximated[11] the class centers and variation around the central values (SLOPE_STD, PLANC_STD and SCI_STD). From Fig. 2.12, we can see that there is quite some confusion between the pits and streams. Other classes seems to be in general easier to distinguish, although there is obviously overlap between streams-plain and ridges-plain. You might try to classify an area using some other generic landforms, such as *pool* or "poolness", *pass*, *saddle* etc. These would, of course, require somewhat different clustering of attribute space (see Fig. 1.9 on page 26). The final classification map can be produced by taking the highest membership per cell (Fig. 2.13). In this case, the most dominant landforms are slopes and plains, while pits occur only in a small portion of the area.

[11] These are empirical values.

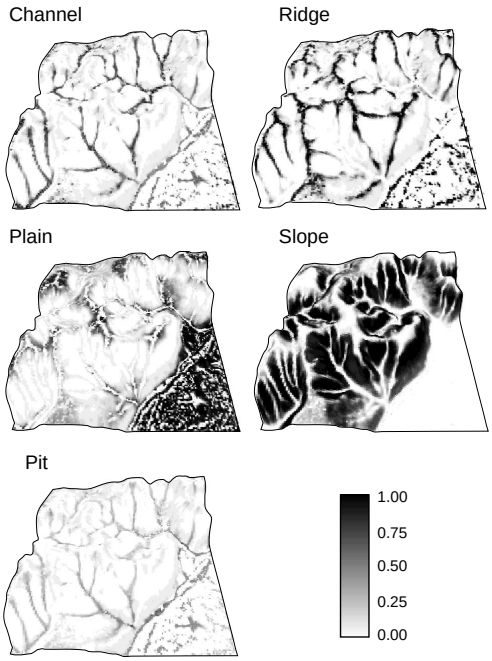

Figure 2.12: Membership maps for five generic landform types.

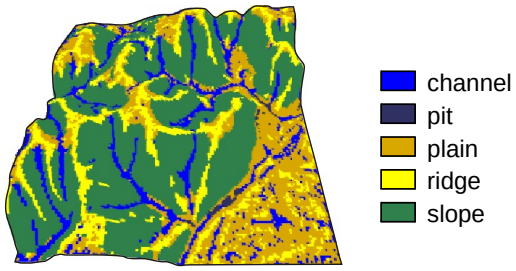

Figure 2.13: Study area classified into the generic landforms.

Table 2.1: SCRIPT: TP_MORPH — Calculation of morpohometric parameters.

	REM: Calculation of morphometric terrain parameters (slope, aspect, curvatures)
1	dx.mpr{dom=value.dom;vr=-500.0000:500.0000:0.0001}=(%1#[3]+%1#[6] +%1#[9]-%1#[1]-%1#[4]-%1#[7])/(6*pixsize(%1))
2	dy.mpr{dom=value.dom;vr=-500.0000:500.0000:0.0001}=(%1#[1]+%1#[2] +%1#[3]-%1#[7]-%1#[8]-%1#[9])/(6*pixsize(%1))
3	//smooth the DEM before deriving second derivatives
4	DEM_s.mpr{dom=value.dom;vr=0.00:5000.00:0.01}=%2*(%1#[1]+%1#[2] +%1#[3]+ %1#[4]+%1#[6]+%1#[7]+%1#[8]+%1#[9])/9+(1-8*%2/9)*%1#[5]
5	//derive second-order derivates and smooth them to get a more generalised picture
6	d2x_tmp.mpr=(DEM_s#[1]+DEM_s#[3]+DEM_s#[4]+DEM_s#[6]+DEM_s#[7] +DEM_s#[9]-2*(DEM_s#[2]+DEM_s#[5]+DEM_s#[8])) /(3*pixsize(DEM_s)^2)
7	d2y_tmp.mpr=(DEM_s#[1]+DEM_s#[2]+DEM_s#[3]+DEM_s#[7]+DEM_s#[8] +DEM_s#[9]-2*(DEM_s#[4]+DEM_s#[5]+DEM_s#[6]))/(3*pixsize(DEM_s)^2)
8	dxy_tmp.mpr=(DEM_s#[3]+DEM_s#[7]-DEM_s#[1]-DEM_s#[9])/ (4*pixsize(DEM_s)^2)
9	d2x{dom=value.dom;vr=-50.0000:50.0000:0.0001}=MapFilter(d2x_tmp, avg3x3)
10	d2y{dom=value.dom;vr=-50.0000:50.0000:0.0001}=MapFilter(d2y_tmp, avg3x3)
11	dxy{dom=value.dom;vr=-50.0000:50.0000:0.0001}=MapFilter(dxy_tmp, avg3x3)
12	//derive slope, aspect, curvatures (filter them for undefined values using iterations)
13	SLOPE.mpr{dom=value.dom;vr=0.0:5000.0:0.1}=100*sqrt(dx^2+dy^2)
14	ASPCT_tmp=raddeg(atan2(dx,dy)+PI)
15	ASPECT{dom=value.dom;vr=0.0:360.0:0.1}= MapIter(ASPCT_tmp.mpr, iff(isundef(ASPCT_tmp), nbprd(ASPCT_tmp#), ASPCT_tmp))
16	PLANC_tmp=-(dy2*d2x-2*dx*dy*dxy+dx^2*d2y)/((dx^2+dy^2)^1.5)*100
17	PLANC{dom=value.dom;vr=-50.000:50.000:0.001}=MapIter(PLANC_tmp.mpr, iff(isundef(PLANC_tmp), nbprd(PLANC_tmp#), PLANC_tmp))
18	PROFC_tmp=-(dx^2*d2x-2*dx*dy*dxy+dy^2*d2y)/((dx^2+dy^2)* (1+dx^2+dy^2)^1.5)*100
19	PROFC{dom=value.dom;vr=-50.000:50.000:0.001}=MapIter(PROFC_tmp.mpr, iff(isundef(PROFC_tmp), nbprd(PROFC_tmp#), PROFC_tmp))
20	MEANC_tmp=-((1+dy^2)*d2x-2*dx*dy*dxy+(1+dx^2)*d2y) /(2*(1+dx^2+dy^2)^1.5)*100
21	MEANC{dom=value.dom;vr=-50.000:50.000:0.001}=MapIter(MEANC_tmp.mpr, iff(isundef(MEANC_tmp), nbprd(MEANC_tmp#), MEANC_tmp))
22	//delete temporary files DEM_s, ????_tmp, d??_tmp

Table 2.2: SCRIPT: FLOW — Calculation of specific catchment area.

	REM: Calculation of specific catchment area
1	S1=iff(isundef(DEM#[1]) OR (DEM<DEM#[1]),0,(DEM-DEM#[1])/4)
2	S2=iff(isundef(DEM#[2]) OR (DEM<DEM#[2]),0,(DEM-DEM#[2])/2)
3	S3=iff(isundef(DEM#[3]) OR (DEM<DEM#[3]),0,(DEM-DEM#[3])/4)
4	S4=iff(isundef(DEM#[4]) OR (DEM<DEM#[4]),0,(DEM-DEM#[4])/2)
5	S6=iff(isundef(DEM#[6]) OR (DEM<DEM#[6]),0,(DEM-DEM#[6])/2)
6	S7=iff(isundef(DEM#[7]) OR (DEM<DEM#[7]),0,(DEM-DEM#[7])/4)
7	S8=iff(isundef(DEM#[8]) OR (DEM<DEM#[8]),0,(DEM-DEM#[8])/2)
8	S9=iff(isundef(DEM#[9]) OR (DEM<DEM#[9]),0,(DEM-DEM#[9])/4)
9	SSUM=S1+S2+S3+S4+S6+S7+S8+S9
10	dA1t{dom=value.dom;vr=0.000:1.000:0.001}=iff(isundef(S1), 0, S1/SSUM)
11	dA2t{dom=value.dom;vr=0.000:1.000:0.001}=iff(isundef(S2), 0, S2/SSUM)
12	dA3t{dom=value.dom;vr=0.000:1.000:0.001}=iff(isundef(S3), 0, S3/SSUM)
13	dA4t{dom=value.dom;vr=0.000:1.000:0.001}=iff(isundef(S4), 0, S4/SSUM)
14	dA6t{dom=value.dom;vr=0.000:1.000:0.001}=iff(isundef(S6), 0, S6/SSUM)
15	dA7t{dom=value.dom;vr=0.000:1.000:0.001}=iff(isundef(S7), 0, S7/SSUM)
16	dA8t{dom=value.dom;vr=0.000:1.000:0.001}=iff(isundef(S8), 0, S8/SSUM)
17	dA9t{dom=value.dom;vr=0.000:1.000:0.001}=iff(isundef(S9), 0, S9/SSUM)
18	dA1=iff(isundef(dA9t#[1]),0,dA9t#[1])
19	dA2=iff(isundef(dA8t#[2]),0,dA8t#[2])
20	dA3=iff(isundef(dA7t#[3]),0,dA7t#[3])
21	dA4=iff(isundef(dA6t#[4]),0,dA6t#[4])
22	dA6=iff(isundef(dA4t#[6]),0,dA4t#[6])
23	dA7=iff(isundef(dA3t#[7]),0,dA3t#[7])
24	dA8=iff(isundef(dA2t#[8]),0,dA2t#[8])
25	dA9=iff(isundef(dA1t#[9]),0,dA1t#[9])
26	start.mpr{dom=value.dom;vr=0.000:50000.000:0.001}=iff(isundef(%1),0,1)
27	ASUM{dom=value.dom;vr=0.00:50000.00:0.01}= MapIter(start.mpr, iff(start<50000, dA1*start#[1]+dA2*start#[2]+dA3*start#[3]+dA4*start#[4] +dA6*start#[6]+dA7*start#[7]+dA8*start#[8]+dA9*start#[9]+1, start),%3)
28	LSUM{dom=value.dom;vr=0.0:10000.0:0.1}=pixsize(%1)*(sqrt(2)/4*(iff(dA1>0,1,0)+iff(dA3>0,1,0)+iff(dA7>0,1,0)+iff(dA9>0,1,0)) + 0.5*(iff(dA2>0,1,0)+iff(dA4>0,1,0)+iff(dA6>0,1,0)+iff(dA8>0,1,0)))
29	CATCH_tmp{dom=value.dom;vr=0.00:50000.00:0.01}=ASUM*pixarea(DEM)/LSUM
30	CATCH=MapIterProp(CATCH_tmp.mpr,iff(isundef(CATCH_tmp) and not(isundef(%2)), nbprd(CATCH_tmp#),CATCH_tmp))
31	//delete temporary files S?, SSUM_tmp, dA?_t, start

Table 2.3: SCRIPT: `GLF_fkm` — Automated extraction of generic landforms using fuzzy k-means.

	REM: Fuzzy k-means classification of landforms
	//Calculate distances from the central value to the attribute band per each class and standardise them according to the standard deviation
1	t_d11=abs(%4-TBLVALUE(%1, "SLOPE", 1))/TBLVALUE(%1, "SLOPE_STD", 1)
2	t_d12=abs(%5-TBLVALUE(%1, "PLANC", 1))/TBLVALUE(%1, "PLANC_STD", 1)
3	t_d13=abs(%6-TBLVALUE(%1, "SCI", 1))/TBLVALUE(%1, "SCI_STD", 1)
4	t_d21=abs(%4-TBLVALUE(%1, "SLOPE", 2))/TBLVALUE(%1, "SLOPE_STD", 2)
5	t_d22=abs(%5-TBLVALUE(%1, "PLANC", 2))/TBLVALUE(%1, "PLANC_STD", 2)
6	t_d23=abs(%6-TBLVALUE(%1, "SCI", 2))/TBLVALUE(%1, "SCI_STD", 2)
7	t_d31=abs(%4-TBLVALUE(%1, "SLOPE", 3))/TBLVALUE(%1, "SLOPE_STD", 3)
8	t_d32=abs(%5-TBLVALUE(%1, "PLANC", 3))/TBLVALUE(%1, "PLANC_STD", 3)
9	t_d33=abs(%6-TBLVALUE(%1, "SCI", 3))/TBLVALUE(%1, "SCI_STD", 3)
10	t_d41=abs(%4-TBLVALUE(%1, "SLOPE", 4))/TBLVALUE(%1, "SLOPE_STD", 4)
11	t_d42=abs(%5-TBLVALUE(%1, "PLANC", 4))/TBLVALUE(%1, "PLANC_STD", 4)
12	t_d43=abs(%6-TBLVALUE(%1, "SCI", 4))/TBLVALUE(%1, "SCI_STD", 4)
13	t_d51=abs(%4-TBLVALUE(%1, "SLOPE", 5))/TBLVALUE(%1, "SLOPE_STD", 5)
14	t_d52=abs(%5-TBLVALUE(%1, "PLANC", 5))/TBLVALUE(%1, "PLANC_STD", 5)
15	t_d53=abs(%6-TBLVALUE(%1, "SCI", 5))/TBLVALUE(%1, "SCI_STD", 5)
	//Calculate sum's of distances for each class
16	sum_dc1=t_d11^2+t_d12^2+t_d13^2
17	sum_dc2=t_d21^2+t_d22^2+t_d23^2
18	sum_dc3=t_d31^2+t_d32^2+t_d33^2
19	sum_dc4=t_d41^2+t_d42^2+t_d43^2
20	sum_dc5=t_d51^2+t_d52^2+t_d53^2
	//Calculate fuzzy factors per each class
21	sum_d1=(sum_dc1)^(-1/(%2-1))
22	sum_d2=(sum_dc2)^(-1/(%2-1))
23	sum_d3=(sum_dc3)^(-1/(%2-1))
24	sum_d4=(sum_dc4)^(-1/(%2-1))
25	sum_d5=(sum_dc5)^(-1/(%2-1))
26	sum_d=sum_d1+sum_d2+sum_d3+sum_d4+sum_d5
	//Calculate memberhsips for each class as sum_dc / sum_d
27	GLF_Channel{dom=Value, vr=0.000:1.000:0.001}=sum_d1/sum_d
28	GLF_Ridge{dom=Value, vr=0.000:1.000:0.001}=sum_d4/sum_d
29	GLF_Slope{dom=Value, vr=0.000:1.000:0.001}=sum_d5/sum_d
30	GLF_Plain{dom=Value, vr=0.000:1.000:0.001}=sum_d3/sum_d
31	GLF_Pit{dom=Value, vr=0.000:1.000:0.001}=sum_d2/sum_d
	//delete temporary files t_d??, sum_d?, sum_d??, sum_?

Bibliography

[1] M. Amstrong and P.A. Dowd, editors. *Geostatistical simulations*, volume vol. 7 of *Proceedings of the Geostatistical Simulation Workshop, Fontainebleau, France, 27-28 May*. Kluwer Academic Publishers, Dodrecht, 1993.

[2] J. Banks, editor. *Handbook of Simulation - Principles, Methodology, Advances, Applications, and Practice*. John Wiley & Sons, New York, 1998.

[3] J.C. Bell, R.L. Cunningham, and M.W. Havens. Soil drainage class probability mapping using a soil-landscape model. *Soil Science Society of America Journal*, 58:464–470, 1994.

[4] P.V. Bolstad and T.M. Lillesand. Improved classification of forest vegetation in northern wisconsin through a rule-based combination of soils, terrain, and landsat tm data. *Forest Science*, 38(1):5–20, 1992.

[5] P.A. Burrough and R.A. McDonnell. *Principles of geographical information systems*. Oxford University Press, Oxford, 1998.

[6] P.A. Burrough, P.F.M. van Gaans, and R.A. MacMillan. High-resolution landform classification using fuzzy k-means. *Fuzzy Sets and Systems*, 113:37–52, 2000.

[7] O. Conrad. Digem - software for digital terrain analysis, 2002. URL `http://www.geogr.uni-goettingen.de /pg/saga/digem/`.

[8] J.G. Corripio. Vectorial algebra algorithms for calculating terrain parameters from dems and solar radiation modelling in mountainous terrain. *International Journal of Geographical Information Science*, 17(1):1–23, 2003.

[9] T.P. D'Avelo and R.L. McLeese. Why are those lines placed where they are?: An investigation of soil map recompilation methods. *Soil Survey Horizons*, 39(4):119–126, 1998.

[10] M.C. Dobson, F.T. Ulaby, and L.E. Pierce. Land-cover classification and estimation of terrain attributes using synthetic aperture radar. *Remote Sensing of Environment*, 51(1):199–214, 1995.

[11] R. Dubayah and P.M. Rich. Topographic solar radiation models for gis. *International Journal of Geographical Information Systems*, 9(4):405–419, 1995.

[12] Environmental Modeling Systems Inc. *The Watershed Modeling System (WMS)*. Brigham Young University, Environmental Modeling Research Laboratory (EMRL), 2002.

[13] Environmental Systems Research Institute. *ArcInfo*. Environmental Systems Research Institute, 2001. URL `http://www.esri.com/software/arcinfo/`.

[14] I.S. Evans. An integrated system of terrain analysis and slope mapping. *Zeitschrift fur Geomorphologie (supplements)*, 36:274–295, 1980.

[15] I.S. Evens and N.J. Cox. Relations between land surface properties: altitude, slope and cruvature. In S. Hergarten and H.J. Neugebauer, editors, *Process Modelling and Landform Evolution*, pages 13–45. Springer Verlag, Berlin, 1999.

[16] A.M. Felicisimo. Parametric statistical method for error detection in digital elevation models. *ISPRS Journal of Photogrammetry and Remote Sensing*, 49(4):29–33, 1994.

[17] J.E. Fels. *Modeling and Mapping Potential Vegetation using Digital Terrain Data: applications in the Ellicott Rock Wilderness of North Carolina, South Carolina, and Georgia*. Phd thesis, North Carolina State University, 1994.

[18] I.V. Florinsky. Accuracy of local topographic variables derived from digital elevation models. *International Journal of Geographical Information Science*, 12(1):47–62, 1998.

[19] I.V. Florinsky, R.G. Eilers, G. Manning, and L.G. Fuller. Prediction of soil properties by digital terrain modelling. *Environmental Modelling and Software*, 17:295–311, 2002.

[20] D.A. Fogg. Contour to rectangular grid conversion using minimum curvature. *Computer Vision, Graphics, and Image Processing*, 28(1):85–91, 1984.

[21] J. Franklin. Predictive vegetation mapping: geographic modeling of biospatial patterns in relation to environmental gradients. *Progress in Physical Geography*, 19:474–499, 1995.

[22] J.C. Gallant and J.P. Wilson. Tapes-g: a grid-based terrain analysis program for the environmental sciences. *Computers & Geosciences*, 22(7):713–722, 1996.

[23] K.F. Gauss. Disquisitiones generales circa area superficies curvas. *Gott. gel. Anz.*, No. 177: 1761–1768, 1827.

[24] P.E. Gessler, I.D. Moore, N.J. McKenzie, and P.J. Ryan. Soil-landscape modelling and spatial prediction of soil attributes. *International Journal of Geographical Information Systems*, 9(4): 421–432, 1995.

[25] B.G.H. Gorte and W. Koolhoven. Interpolation between isolines based on the borgefors distance transform. *ITC Journal*, 1(3):245–247, 1990.

[26] Helios Environmental Modeling Institute. Topoview 1.1, user manual, 1999. URL `http://www.hemisoft.com/topoview/manual/`.

[27] T. Hengl, S. Gruber, and D.P. Shrestha. Reduction of errors in digital terrain parameters used in soil-landscape modelling. *International Journal of Applied Earth Observation and Geoinformation (JAG)*, in review, 2003.

[28] G.B.M. Heuvelink. *Error propagation in quantitative spatial modelling*. Phd thesis, University of Utrecht, 1994.

[29] M. Hiroko and A. Masamu. Use of contour-based dems for deriving and mapping topographic attributes. *Photogrammetric Engineering & Remote Sensing*, 68(1):83–93, 2002.

[30] K.W. Holmes, O.A. Chadwick, and Ph.C. Kyriakidis. Error in a `USGS` 30m digital elevation model and its impact on digital terrain modeling. *Journal of Hydrology*, 233:154–173, 2000.

[31] B.K.P. Horn. Hill shading and the reflectance map. *Proceedings IEEE*, 69(1):14–47, 1981.

[32] D. Houlder, M. Hutchinson, H. Nix, and J. McMahon. *ANUCLIM user's guide*. Centre for Resource and Environmental Studies, Australian National University, Canberra, 2000.

[33] M.F. Hutchinson. A new procedure for gridding elevation and stream line data with automatic removal of spurious pits. *Journal of Hydrology*, 106:211–232, 1989.

[34] B.J. Irvin, S.J. Ventura, and B.K. Slater. Fuzzy and isodata classification of landform elements from digital terrain data in pleasant valley, wisconsin. *Geoderma*, 77:137–154, 1997.

[35] E.H. Isaaks and R.M. Srivastava. *Applied Geostatistics*. Oxford University Press, New York, 1989.

[36] A.J. Izenman. Recent developments in nonparametric density estimation. *Journal of the American Statistical Association*, 86(413):205–224, 1991.

[37] I.S. Kweon and T. Kanade. Extracting topographic terrain features from elevation maps. *Computer Vision Graphics and Image Processing Journal*, 59(2):171–182, 1994.

[38] S.N. Lane, K.S. Richards, and J.H. Chandler. *Landform monitoring, modelling and analysis.* John Wiley and Sons, 1998.

[39] Z. Li. A comparative study of the accuracy of digital terrain models (dtms) based on various data models. *ISPRS Journal of Photogrammetry and Remote Sensing*, 49:2–11, 1994.

[40] R.A. MacMillan, W.W. Pettapiece, S.C. Nolan, and T.W. Goddard. A generic procedure for automatically segmenting landforms into landform elements using dems, heuristic rules and fuzzy logic. *Fuzzy Sets and Systems*, 113:81–109, 2000.

[41] D.M. Mark. Geomorphometric parameters: a review and evaluation. *Geografiska Annaler*, 57A (3-4):165–177, 1975.

[42] D. Martinoni. *Models and Experiments for Quality Handling in Digital Terrain Modelling*. Phd thesis, University of Zurich, 2002.

[43] L.W. Martz and E. de Jong. Catch: a fortran program for measuring catchment area from digital elevation models. *Computers and Geosciences*, 14(5):627–640, 1988.

[44] C.L. Miller and R.A. Laflamme. The digital terrain model - theory and application. *Photogrammetric Engineering*, 24(3):433–442, 1958.

[45] L. Mitas and H. Mitasova. Spatial interpolation. In P. Longley, M.F. Goodchild, D.J. Maguire, and D.W. Rhind, editors, *Geographical Information Systems: Principles, Techniques, Management and Applications*, volume 1, pages 481–492. Wiley, 1999.

[46] H. Mitasova and J. Hofierka. Interpolation by regularized spline with tension, ii application to terrain modelling and surface geometry analysis. *Mathematical Geology*, 25:657–669, 1993.

[47] H. Mitasova, J. Hofierka, M. Zlocha, and L. R. Iverson. Modelling topographic potential for erosion and deposition using gis. *International Journal of Geographical Information Systems*, 10(5):629–641, 1996.

[48] H. Mitasova, L. Mitas, W.M. Brown, D.P. Gerdes, I. Kosinovsky, and T. Baker. Modeling spatially and temporally distributed phenomena: New methods and tools for grass gis. *International Journal of Geographical Information Systems*, 9(4):433–446, 1995.

[49] I.D. Moore, P.E. Gessler, G.A. Nielsen, and G.A. Peterson. Soil attribute prediction using terrain analysis. *Soil Science Society of America Journal*, 57(2):443–452, 1993.

[50] I.D. Moore, R.B. Grayson, and A.R. Ladson. Digital terrain modelling: a review of hydrological, geomorphological, and biological applications. *Hydrological Processes*, 5(1):3–30, 1991.

[51] NASA. Shuttle Radar Topography Mission, 2002.

[52] D.J. Pennock, B.J. Zebarth, and E. de Jong. Landform classification and soil distribution in hummocky terrain, sasketchewan, canada. *Geoderma*, 40:297–315, 1987.

[53] T.K. Peucker, R.J. Fowler, J.J. Little, and D.M. Mark. The triangulatd irregular network. In *Proceedings of the ASP Digital Terrain Models (DTM) Symposium*, pages 516–540, Falls Church Virginia, 1978. American Society of Photogrammetry.

[54] M. Pilouk. *Fidelity improvement of DTM from contours.* Msc thesis, ITC, 1992.

[55] M. Pilouk and K. Tempfli. A digital image processing approach to creating dtms from digitized contours. *International Archives of Photogrammetry and Remote Sensing*, 29(B4):956961, 1992.

[56] P. Quinn, K. Beven, P. Chevallier, and O. Planchon. The prediction of hillslope flow paths for distributed hydrological modelling using digital terrain models. *Hydrological processes*, 5: 59–79, 1991.

[57] L. Raaflaub and M.J. Collins. The effect errors in gridded digital elevation have on derived topographic parameters using monte carlo simulation: A comparison of algorithms. In Gary J. Hunter and Kim Lowell, editors, *Proceedings of the 5th International Symposium on Spatial Accuracy Assesment in Natural Resources and Environmental Sciences (Accuracy 2002)*, page 279, Melbourne, Australia, 2002.

[58] D.G. Rossiter. *Methodology for Soil Resource Inventories.* ITC Lecture Notes SOL.27. ITC, Enschede, the Netherlands, 2nd edition, 2001.

[59] D.G. Rossiter and T. Hengl. Technical note: Creating geometrically-correct photo-interpretations, photomosaics, and base maps for a project gis. Technical report, ITC, Soil Science Division, 2002.

[60] B. Schneider. *Geomorphologically Plausibel Reconstruction of the Digital Representation of Terrain Surfaces from Contour Data (in german).* Phd thesis, Universtiy of Zurich, 1998.

[61] P.A. Shary, L.S. Sharaya, and A.V. Mitusov. Fundamental quantitative methods of land surface analysis. *Geoderma*, 107(1-2):1–32, 2002.

[62] Golden Software. *Surfer User's Guide*. Golden Software, 2001. URL `http://www.golden.com/frames/surferframe.htm`.

[63] G. Tang, W. Shi, and M. Zhao. Evaluation on the accuracy of hydrologic data derived from dems of different spatial resolution. In Gary J. Hunter and Kim Lowell, editors, *Proceedings of the 5th International Symposium on Spatial Accuracy Assesment in Natural Resources and Environmental Sciences (Accuracy 2002)*, pages 204–213, Melbourne, Australia, 2002.

[64] D.G. Tarboton. A new method for the determination of flow directions and contributing areas in grid digital elevation models. *Water Resources Research*, 33(2):309–319, 1997.

[65] K. Tempfli. Dtm accuracy assesment. In *ASPRS Annual Conference*, pages 1–11, Portland, 1999.

[66] A.L. Thomas, D. King, E. Dambrine, A. Couturier, and J. Roque. Predicting soil classes with parameters derived from relief and geologic materials in a sandstone region of the vosges mountains (northeastern france). *Geoderma*, 90(3-4):291–305, 1999.

[67] J.A. Thompson, J.C. Bell, and C.A. Butler. Quantitative soil-landscape modeling for estimating the areal extent of hydromorphic soils. *Soil Science Society of America Journal*, 61(3): 971–980, 1997.

[68] J.A. Thompson, J.C. Bell, and C.A. Butler. Digital elevation model resolution: effects on terrain attribute calculation and quantitative soil-landscape modeling. *Geoderma*, 100:67–89, 2001.

[69] TopoSys. *TopoSys Topographische Systemdaten GmbH*. TopoSys, Ravensburg, Germany, 2002. URL `http://www.toposys.com`.

[70] Understanding Systems Inc. Oasis: Topometrix, documentation, 1999. URL `http://www.undersys.com`.

[71] Unit Geo Software Development. *ILWIS 3.0 Academic user's guide*. ITC, Enschede, 2001.

[72] USGS - NASA Distributed Active Archive Centre. *FTP access to Global AVHRR 10-day composite data*. US Geological Survey, 2001. URL `http://edcdaac.usgs.gov/1KM/comp10d.html`.

[73] A.P.A. Vink. *Land use in advancing agriculture*, volume x. Springer-Verlag, New York, 1975.

[74] R. Weibel and M. Heller. Digital terrain modelling. In D.J. Maguire, M.F. Goodchild, and D.W. Rhind, editors, *Geographical information systems*, volume 1, pages 269–297. Longman, London, 1991.

[75] J.P. Wilson and J.C. Gallant. Eros: a grid-based program for estimating spatially distributed erosion indices. *Computers and Geosciences*, 22:707–712, 1996.

[76] J.P. Wilson and J.C. Gallant, editors. *Terrain analysis: principles and applications*. John Wiley & Sons, Ltd., New York, 2000.

[77] J.P. Wilson, P.L. Repetto, and R.D. Snyder. Effect of data source, grid resolution, and flow-routing method on computed topographic attributes. In John P. Wilson and John C. Gallant, editors, *Terrain Analysis: Principles and Applications*, pages 133–161. John Wiley & Sons, Inc., 2000.

[78] S.M. Wise. Assessing the quality for hyrdological applications of digital elevation models derived from contours. *Hydrological Processes*, 14(11-12):1909–1929, 2000.

[79] J. Woo. *The Geomorphological Characterisation of Digital Elevation Models*. Phd thesis, University of Leicester, 1996.

[80] J. Woo. Landserf: Visualisation and analysis of terrain models, 2001. URL `http://www.geog.le.ac.uk/jwo/`.

[81] M. Young. Terrain analysis: program documentation, 1978.

[82] H.A. Zebker, C.L. Werner, P.A. Rosen, and S. Hensley. Accuracy of topographic maps derived from ers-1 interferometric radar. *IEEE Transactions on Geoscience and Remote Sensing*, 32 (4):823–836, 1994.

[83] L.W. Zevenbergen and C.R. Thorne. Quantitative analysis of land surface topography. *Earth Surface Processes Landforms*, 12:47–56, 1987.

[84] Q. Zhou and X. Liu. Error assessment of grid-based flow routing algorithms used in hydrological models. *International Journal of Geographical Information Science*, 16(8):819–842, 2002.